Automatica 123 (2021) 109330

Contents lists available at ScienceDirect

Automatica

journal homepage: www.elsevier.com/locate/automatica

Multi-competitive viruses over time-varying networks with mutations and human awareness☆

Philip E. Paré [a,*], Ji Liu [b], Carolyn L. Beck [c], Angelia Nedić [d], Tamer Başar [c]

[a] School of Electrical and Computer Engineering, Purdue University, West Lafayette, IN, United States of America
[b] Department of Electrical and Computer Engineering, Stony Brook University, NY, United States of America
[c] Coordinated Science Laboratory, ECE Department, University of Illinois at Urbana–Champaign, IL, United States of America
[d] School of Electrical, Computer and Energy Engineering, Arizona State University, AZ, United States of America

ARTICLE INFO

Article history:
Received 27 August 2019
Received in revised form 11 August 2020
Accepted 17 September 2020
Available online 18 November 2020

ABSTRACT

In this paper, we introduce a model for multiple competing viruses over networks, derived using each state variable of the model as the infection percentage of a group or a subpopulation. We show that the model is well-posed, and also compare it to a full probabilistic Markov model. We provide a necessary and sufficient condition for uniqueness of the healthy state (the origin) of the multi-virus model over static graphs. We also provide several sufficient conditions for convergence to the healthy state for mutating viruses over dynamic networks. We analyze various endemic states of the multi-virus model over static graphs, including providing necessary and sufficient conditions for the existence of parallel equilibria. We further extend the model to include an awareness state, allowing nodes to become alerted to the fact that viruses are spreading in the system and therefore reduce their susceptibility, and analyze the equilibria of such a model. Finally, we propose several antidote control techniques and present a set of illustrative simulations.

1. Introduction

Spread dynamics have been studied for hundreds of years; Bernoulli developed one of the first known models inspired by the smallpox virus (Bernoulli, 1760). The importance of this problem has been highlighted recently by the COVID-19 pandemic, which spread across the world due to time-varying connections (Dong et al., 2020) and a possibly mutating virus. In this paper, we focus exclusively on susceptible–infected–susceptible (SIS) epidemiological models, which have been developed for both continuous (Ahn & Hassibi, 2013; Fall et al., 2007; Kermack & McKendrick, 1932; Mieghem et al., 2009) and discrete time domains (Ahn & Hassibi, 2013; Peng et al., 2010; Wang et al., 2003). SIS models consist of multiple agents, or subpopulations, that are either infected or healthy (susceptible) at any time t, and which may cycle (aperiodically) between these two states. The rate of infection combined with the connectivity of the ith agent to an infected neighbor j (denoted by β_{ij}) positively affects the probability of being infected, or proportion of the infected subpopulation, while the healing rate δ_i negatively affects the infection probability, or proportion of the infected subpopulation. This dynamic is depicted in Fig. 1(a). In this work, we focus on the group/subpopulation interpretation.

Competitive virus models, where each node can be infected by only one spreading process, have been motivated in the literature by competing viral strains (Nowak, 1991) and incompatible ideas spreading on different social networks (Sahneh & Scoglio, 2014), but they can also have broader applications to adoption of competing products, political stances, and alternative farming practices. The idea of two competitive SIS viruses, namely the bi-virus model, has been recently pursued in Karrer and Newman (2011), Liu et al. (2016, 2019), Nowak (1991), Prakash et al. (2012), Sahneh and Scoglio (2014), Santos et al. (2015), Watkins et al. (2016) and Wei et al. (2013). Competitive SIS models were first introduced by Nowak in Nowak (1991), which is an extension of Kermack and McKendrick (1932), where the model considers the dynamics of three groups: (1) susceptible, (2) infected by virus one, and (3) infected by virus two. These dynamics were modeled using three differential equations where full connectivity of the agents is assumed (i.e., the infection graph

☆ This material is based on research partially supported by the National Science Foundation, grants ECCS 15-09302, CNS 15-44953, ECCS 2032258, and ECCS 2032321, and the Jump ARCHES endowment through the Health Care Engineering Systems Center of the University of Illinois at Urbana-Champaign. All material in this paper represents the position of the authors and not necessarily that of NSF. The material in this paper was partially presented at the 2017 American Control Conference, May 24–26, 2017, Seattle, WA, USA. This paper was recommended for publication in revised form by Associate Editor Vijay Gupta under the direction of Editor Christos G. Cassandras.

* Corresponding author.
E-mail addresses: philpare@purdue.edu (P.E. Paré), ji.liu@stonybrook.edu (J. Liu), beck3@illinois.edu (C.L. Beck), angelia.nedich@asu.edu (A. Nedić), basar1@illinois.edu (T. Başar).

https://doi.org/10.1016/j.automatica.2020.109330
0005-1098/

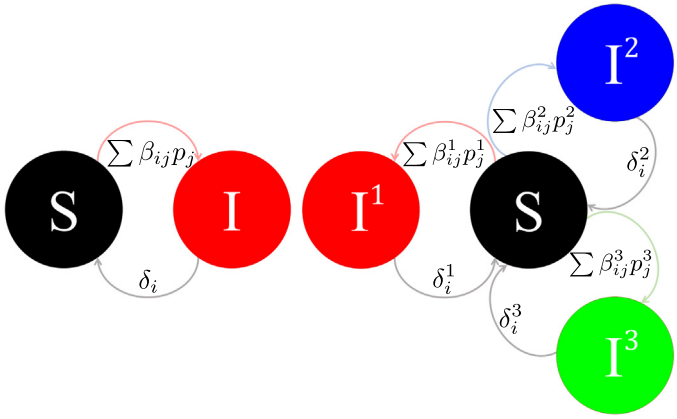

(a) SIS Model. (b) Three Competing Viruses.

Fig. 1. The *i*th node can be either in a susceptible or an infected condition (the summations are over *j*).

is a complete graph), and where both viruses are assumed to be homogeneous. A virus is *homogeneous* if all agents have the same infection rate and healing rate. Otherwise, the virus is referred to as *heterogeneous*. In Watkins et al. (2016), Watkins et al. provide a necessary and sufficient condition for local exponential stability of the origin for two competing heterogeneous viruses over strongly connected graphs. In addition, a geometric programming problem is formulated, working toward optimal stabilization and rate control of the viruses. In Liu et al. (2016, 2019), Liu et al. provide global analysis for healthy and endemic states for the bi-virus model over strongly connected graphs and investigate distributed control techniques. The idea of information diffusion on two layered networks has also been explored using a susceptible–infected–recovered (SIR) model in Yagan et al. (2013). Additional two-virus work can be found in Ahn et al. (2006) and Funk and Jansen (2010).

The main motivations for studying the bi-virus model are those of competing viral strains (Nowak, 1991) and competing ideas spreading on different social networks (Sahneh & Scoglio, 2014). However, these models have broader applications to political stances, adaptation of competing products, competing practices in farming, etc., and can be generalized to more than two viruses. Consider, for example, the case of three competing viruses, for which each node has four possible conditions: susceptible, infected by virus 1, 2, or 3. This scenario is depicted in Fig. 1(b).

To the best of our knowledge, the only work that has considered more than two competing SIS viruses is presented in Xu et al. (2012), where Xu et al. propose a multi-virus model to capture the behavior of the spread of computer viruses. This model is different than the model we consider herein, in that it allows viruses to "rob" each other and requires the viruses to spread on the same static graph. In addition, the analysis presented in Xu et al. (2012) considers only the healthy state.

The modeling of mutating viruses has previously been addressed in Gubar and Zhu (2013), Kutch and Gurfil (2002) and Singh (2006). In Kutch and Gurfil (2002), Kutch and Gurfil introduce differential equations describing infection by viruses immune to different HIV drugs. In Singh (2006), Singh models virus mutation using the addition of another virus. In Gubar and Zhu (2013), Gubar and Zhu use evolutionary dynamics to model the virus mutations. To the best of our knowledge no work has been done on studying mutating viruses over nontrivial networks. In this work we model the mutating viruses by allowing the infection and healing rates to change over time, which we believe is novel.

Previous work on competing viruses has focused on non-mutating viruses over static graph structures, which we posit are not realistic given the dynamic nature of human contact networks. There are also recent results for single-virus models over time-varying networks (Bokharaie et al., 2010; Paré et al., 2015, 2018; Prakash et al., 2010; Rami et al., 2014; Schwarzkopf et al., 2010). Some of the ideas from Paré et al. (2018) will be employed in this paper and applied to a more general model. Additional work on virus spread over dynamic graph structures can be found in Fefferman and Ng (2007) and Volz and Meyers (2009).

Given an active outbreak, since agents in a population communicate with each other, it is possible they become *aware* of the virus and change their behavior in order to reduce susceptibility, which has been seen with the recent COVID-19 pandemic and social distancing (Lewnard & Lo, 2020). Virus spread models that account for human awareness have been studied in Funk et al. (2009), Granell et al. (2013), Liu et al. (2017), Ogura and Preciado (2016), Paarporn et al. (2017), Sahneh and Scoglio (2011, 2012) and Shakeri et al. (2015). The only work that includes human awareness with competing viruses is Liu et al. (2017), where only the bi-virus case is considered. In this work, we extend our results from Liu et al. (2017) to a more general scenario, which incorporates human awareness with multi-virus models.

Mathematical models of viruses are studied in order to understand the spreading behavior and to develop suppression and mitigation strategies that minimize the impact of outbreaks. Various control techniques have been applied to SIS virus systems (Liu et al., 2019; Vijayshankar & Roy, 2012; Wan et al., 2007, 2008; Watkins et al., 2016); these techniques regard the healing rate as a control variable. In Liu et al. (2019), it is shown that there exists no distributed linear feedback control that can stabilize the system, and in fact, such a control structure will destabilize the system. Alternative approaches focus on reducing the maximum eigenvalue of the linearized system using the healing rate and/or the infection rate. In Wan et al. (2007, 2008), distributed control techniques for setting healing rate and quarantine protocols are proposed and implemented on a severe acute respiratory syndrome (SARS) simulation model. In Vijayshankar and Roy (2012), a bound is provided for the cost of fairness of mitigating the spread of disease, that is, the difference between the optimal solution and the fair or homogeneous solution, for several classes of graphs. In Preciado et al. (2014), geometric programming ideas are used to control single SIS virus systems and the authors present a polynomial time algorithm illustrated on an air transportation network. In Watkins et al. (2016), ideas similar to those in Preciado et al. (2014) are applied to the bi-virus model. In Pasqualetti et al. (2014), a network control technique is applied to a discretized, linearized version of the model from Mieghem et al. (2009).

1.1. Paper contributions

In this paper, we present a generalization of the bi-virus model from Liu et al. (2019) to include an arbitrary finite number of competing viruses, which is represented by a set of m ordinary differential equations (ODEs). We provide conditions for stability of the *healthy state*, where all viruses are eradicated, for competing viruses over static graphs as well as for mutating competing viruses over time-varying graph structures. We also explore the endemic states of the model by (1) providing sufficient conditions for stability of the case when only one virus survives, and (2) providing a necessary and sufficient condition for the existence of parallel endemic states, meaning the equilibrium for each virus is a scaled version of the others. In order to capture more realistic behavior, we extend the model to incorporate human awareness,

show that the extended model is well defined, determine the equilibria where the virus is eradicated, and present a set of sufficient conditions for the healthy states. Leveraging the stability results, we provide two control techniques based on minimizing the maximum eigenvalue of the linearized system. These control techniques, which are different from previous approaches in the literature, allow every agent to have a base healing rate and an additive control term. The corollaries, theorems, and control techniques are then illustrated via simulations.

Some of the material in this paper was partially presented earlier in Paré et al. (2017); this paper provides a more comprehensive treatment of the work, expands to the case of mutating viruses, and includes human awareness. Specifically, the paper provides (1) a derivation of the multi-virus model in Section 2, interpreting each state variable of the model as the infection proportion of a group or subpopulation; (2) a presentation of the full probabilistic $(m+1)^n$ state model with a comparison to the ODE model via simulations; (3) complete proofs of all the results; (4) a new parallel equilibrium result (Theorem 6) that is both necessary and sufficient, including a generalization of earlier results only shown to be sufficient but herein proven to be necessary as well; (5) an extension of the model to include human awareness; (6) a relaxation of the control problems, no longer requiring a symmetric graph; and (7) additional illustrative simulations in Section 7, none which was included in Paré et al. (2017). The mutating, time-varying results in Section 3.2 are extensions of the single-virus work presented in Paré et al. (2018), but are extended to the case with mutating (time-varying) virus parameters. The analysis of the endemic states in Section 4 is based on extensions of the work in Liu et al. (2016, 2019); therefore we state some of the results as corollaries. The novelty in the work presented herein is the extension of the model to an arbitrary number of competing viruses and to capture mutating viruses and human awareness, and the proposed control techniques in Section 6.

The paper is organized as follows. We first introduce in Section 2 the SIS model and derive the competing virus model for m viruses. In Sections 3 and 4 , we analyze the model, providing conditions for stability of the healthy state and the endemic states. In Section 5 we extend the multi-virus model to include human awareness and provide results on stability of the healthy states, and in Section 6, we provide an antidote control formulation. In Section 7, we present a set of illuminating simulations of various competing virus models over static and time-varying networks. We conclude in Section 8.

1.2. Notation

For any positive integer n, we use $[n]$ to denote the set $\{1, 2, \ldots, n\}$. We view vectors as column vectors. We use x^T and $\|x\|$ to denote the transpose and the 2-norm of a vector x, respectively. The ith entry of a vector x will be denoted by x_i. The ijth entry of a matrix A will be denoted by a_{ij}, and also by $[A]_{ij}$ when convenient. We use $\mathbf{0}$ and $\mathbf{1}$ to denote the vectors whose entries are all 0 and 1, respectively, and I to denote the identity matrix; dimensions of vectors and matrices are to be understood from the context. For any vector $x \in \mathbb{R}^n$, we use $\mathrm{diag}(x)$ to denote the $n \times n$ diagonal matrix whose ith diagonal entry is x_i. For any two sets $\mathcal{A}$ and $\mathcal{B}$, we use $\mathcal{A} \setminus \mathcal{B}$ to denote the set of elements in $\mathcal{A}$ but not in $\mathcal{B}$.

For any two real vectors $a, b \in \mathbb{R}^n$, we write $a \geq b$ if $a_i \geq b_i$ for all $i \in [n]$, $a > b$ if $a \geq b$ and $a \neq b$, and $a \gg b$ if $a_i > b_i$ for all $i \in [n]$. For a real square matrix M, we use $s(M)$ to denote the largest real part among its eigenvalues, i.e., $s(M) = \max\{\mathrm{Re}(\lambda) : \lambda \in \sigma(M)\}$, where $\mathrm{Re}(\cdot)$ is the real part of the argument and $\sigma(M)$ denotes the spectrum of M, and $\|M\|$ indicates the induced 2-norm of M (the maximum singular value of M). For a symmetric matrix M, we use $\lambda_1(M)$ to denote its largest eigenvalue. The notation $1_{a=b}$ denotes the indicator function which takes value one if a equals b and zero otherwise. For $1_{A=b}$, where A is a matrix and b is a scalar, the result is a binary matrix of the same dimensions as A with entries $1_{a_{ij}=b}$.

2. The model

The generic SIS model is a generalization of models introduced in Fall et al. (2007) and Mieghem et al. (2009), given by

$$\dot{p}_i(t) = (1 - p_i(t)) \sum_{j=1}^{n} \beta_{ij} p_j(t) - \delta_i p_i(t), \tag{1}$$

where p_i can be interpreted as the proportion of infected individuals in group i (Fall et al., 2007) or as the probability that agent i is infected (Mieghem et al., 2009), the β_{ij}'s are (possibly asymmetric) infection rates incorporating the nearest-neighbor graph structure, and δ_i is the healing rate. Neighbor relationships among the n nodes are described by a directed graph $\mathbb{G}$ on n vertices with an arc from vertex j to vertex i whenever node i can be infected by node j. The nodes can be thought of as single individuals, or as groups of people in which case the neighbor graph $\mathbb{G}$ can have self-arcs at all n vertices. Hence, β_{ij} equals zero if there is no edge in $\mathbb{G}$ from node j to node i.

This model has been extended to two viruses and studied in Liu et al. (2016), Sahneh and Scoglio (2014) and Santos et al. (2015). We need not restrict ourselves to two viruses, however. We are interested in the following continuous-time distributed model for m competing viruses. Consider a network consisting of $n > 1$ groups of individuals, labeled 1 to n. There are m competing viruses spreading over the network. An individual can be infected with at most one virus at any time t. An individual may be infected with one of the viruses, but only by those in its own and neighboring groups. Neighbor relationships among the n groups are described by a directed graph $\mathbb{G}$ on n vertices with an arc from vertex j to vertex i whenever the individuals in group i can be infected by those in group j. Thus, the neighbor graph $\mathbb{G}$ has self-arcs at all n vertices and the directions of arcs in $\mathbb{G}$ represent the directions of contagion. Each virus spreads over a spanning subgraph of $\mathbb{G}$. The m subgraphs can be different. Their union is the neighbor graph $\mathbb{G}$. It is assumed that each of the m subgraphs is strongly connected, that is, for every pair of distinct vertices i and j, there is a directed path from i to j in the graph, and, thus, so is $\mathbb{G}$.

Let $S_i(t)$ denote the number of susceptible individuals in group i at time $t \geq 0$, and, for every $k \in [m]$, let $I_i^k(t)$ denote the number of individuals infected by virus k in group i at time $t \geq 0$. Assume the total number of individuals in each group i, denoted by N_i, does not change over time. In other words, $S_i(t) + \sum_{k=1}^{m} I_i^k(t) = N_i$, for all $i \in [n]$ and $t \geq 0$. Several parameters are associated with each group i: birth rate μ_i, death rate $\bar{\mu}_i$, and healing rates γ_i^k and infection rates α_{ij}^k for every virus $k \in [m]$, $i, j \in [n]$. Since N_i is constant, $\bar{\mu}_i = \mu_i$. The evolution of the number of infected and susceptible individuals in each group i is as follows:

$$\begin{aligned}\dot{S}_i(t) &= \mu_i N_i - \bar{\mu}_i S_i(t) + \sum_{k=1}^{m} \gamma_i^k I_i^k(t) - \sum_{k=1}^{m} \sum_{j=1}^{n} \alpha_{ij}^k \frac{S_i(t)}{N_i} I_j^k(t) \\ &= \sum_{k=1}^{m} (\mu_i + \gamma_i^k) I_i^k(t) - \sum_{k=1}^{m} \sum_{j=1}^{n} \alpha_{ij}^k \frac{S_i(t)}{N_i} I_j^k(t),\end{aligned} \tag{2}$$

and for every virus $k \in [m]$,

$$\dot{I}_i^k(t) = -\gamma_i^k I_i^k(t) - \bar{\mu}_i I_i^k(t) + \sum_{j=1}^{n} \alpha_{ij}^k \frac{S_i(t)}{N_i} I_j^k(t)$$
$$= (-\gamma_i^k - \mu_i) I_i^k(t) + \sum_{j=1}^{n} \alpha_{ij}^k \frac{S_i(t)}{N_i} I_j^k(t). \quad (3)$$

To simplify the model, for every virus $k \in [m]$, define the proportion of infected individuals in group i by

$$p_i^k(t) = \frac{I_i^k(t)}{N_i},$$

and let

$$\beta_{ij}^k = \alpha_{ij}^k \frac{N_j}{N_i}, \quad \delta_i^k = \gamma_i^k + \mu_i.$$

From (3), it follows that for every virus $k \in [m]$,

$$\dot{p}_i^k(t) = (1 - p_i^1(t) - \cdots - p_i^m(t)) \sum_{j=1}^{n} \beta_{ij}^k p_j^k(t) - \delta_i^k p_i^k(t). \quad (4)$$

The competition feature of the model is captured by the first term where if agent i is infected completely with virus l, i.e., $p_i^l = 1$, then it cannot be infected with any virus $k \neq l$.

This representation can be written in matrix form as:

$$\dot{p}^k(t) = ((I - P^1(t) - \cdots - P^m(t))B^k - D^k)p^k(t), \quad (5)$$

where p^k is the vector of the p_i^k's, B^k is the matrix of the β_{ij}^k's, $P^k = \mathrm{diag}(p^k)$, and $D^k = \mathrm{diag}(\delta_1^k, \ldots, \delta_n^k)$. The set

$$\mathcal{D} = \left\{ (p^1, \ldots, p^m) \mid p^k \geq \mathbf{0}, \ k \in [m], \ \sum_{k=1}^{m} p^k \leq \mathbf{1} \right\} \quad (6)$$

is invariant with respect to the system defined by (5). By the above derivation where the state variables are representative of the proportion of infected members of a group or subpopulation, it is natural to assume that their initial values are in $[0, 1]$, as otherwise the values will lack any physical meaning for the epidemic model considered herein. Alternatively, if p_i^k denotes the probability of infection of agent i by virus k and $1 - \sum_{k=1}^{m} p_i^k$ denotes the probability of agent i being healthy, the state variables should also be bounded between zero and one. Note that the group interpretation allows for self loops in the model while the individual probabilistic interpretation does not Paré et al. (2018). For completeness, we provide a full description of the $(m+1)^n$ state Markov model in the Appendix. We now show that (4) is well-defined.

Lemma 1. *Suppose that for all $i \in [n]$, $k \in [m]$, we have $\delta_i^k \geq 0$, and the matrices B^k are non-negative. If for all $i \in [n]$, $k \in [m]$, we have $p_i^k(0), (1 - p_i^1(0) - \cdots - p_i^m(0)) \in [0, 1]$, then $p_i^k(t), p_i^1(t) + \cdots + p_i^m(t) \in [0, 1]$ for all $i \in [n]$, $k \in [m]$ and $t \geq 0$.*

Proof. Suppose that at some time τ, $p_i^1(\tau) + \cdots + p_i^m(\tau) \in [0, 1]$ and $p_i^k(\tau) \in [0, 1]$ for all $i \in [n], k \in [m]$. Consider an index $i \in [n]$. If $p_i^k(\tau) = 0$, then from (4) and the assumption that the matrices B^k are non-negative, $\dot{p}_i^k(\tau) \geq 0$. The same holds for $p_i^1(\tau) + \cdots + p_i^m(\tau)$. If $p_i^k(\tau) = 1$, then from (4) and the assumption that the matrices B^k are non-negative, $\dot{p}_i^1(\tau) \leq 0$. The same holds for $p_i^1(\tau) + \cdots + p_i^m(\tau)$. It follows that $p_i^k(t), p_i^1(t) + \cdots + p_i^m(t) \in [0, 1]$ for all $i \in [n], k \in [m]$ and $t \geq \tau$. Since, by assumption, $p_i^k(0), (1 - p_i^1(0) - \cdots - p_i^m(0)) \in [0, 1]$ for all $i \in [n], k \in [m]$, it follows that $p_i^k(t), p_i^1(t) + \cdots + p_i^m(t) \in [0, 1]$ for all $i \in [n], k \in [m]$ and $t \geq 0$. □

Henceforth we assume $p_i^k(0), (1 - \sum_j^m p_i^j(0)) \in [0, 1]$ for all $i \in [n], k \in [m]$.

It has been shown that there are a healthy state equilibrium and endemic equilibria for the single-virus system (Khanafer et al., 2014, 2016; Paré et al., 2015, 2018), as well as for the two-virus system (Liu et al., 2019). The multi-virus case is similar, although more complicated because all viruses can reach the healthy state, or an endemic state, or there may be some viruses at a healthy state and some at an endemic state. We explore several conditions for convergence to these equilibria.

3. Stability analysis of the healthy state

We provide conditions for the stability of the healthy state for both the non-mutating, static graph case, and the mutating, dynamic graph case. For results on non-mutating viruses over static graphs, we assume that the B^k matrices are irreducible. This assumption implies that the underlying graph is strongly connected, that is, there is a directed path from every node to every other node in the graph. Note that this assumption is not made in the case of mutating viruses over time-varying graphs.

3.1. Static non-mutating case

In the following we consider the non-mutating, static graph version of the system defined by the state equations given in (4). We first give conditions under which the healthy state is asymptotically stable.

Lemma 2. *Suppose for all $i \in [n], k \in [m]$, we have $\delta_i^k \geq 0$ and matrices B^k are non-negative and irreducible. If $s(B^k - D^k) \leq 0$ for all $k \in [m]$, then the healthy state is the unique equilibrium of (5), which is asymptotically stable with domain of attraction $\mathcal{D}$ defined in (6).*

Proof. To prove the lemma, it is sufficient to show that for all $k \in [m]$, $p^k(t)$ will asymptotically converge to $\mathbf{0}$ as $t \to \infty$ for any initial condition.

Since for all $k \in [m]$, $p_i^k(t)$ is always non-negative by Lemma 1, from (4) it follows that

$$\dot{p}_i^1(t) \leq -\delta_i^1 p_i^k(t) + (1 - p_i^k(t)) \sum_{j=1}^{n} \beta_{ij}^k p_j^1(t), \quad (7)$$

which implies that the trajectories of $p_i^k(t)$ are bounded above by those of the single-virus model. Since matrices B^k are non-negative and irreducible, by Proposition 2 in Liu et al. (2019), $p^k(t)$ will asymptotically converge to $\mathbf{0}$ as $t \to \infty$ for all $k \in [m]$. Thus, the healthy state is the unique equilibrium of (5). □

We now show the condition in Lemma 2 is necessary and sufficient for eradication of all viruses.

Theorem 1. *Suppose $\delta_i^k \geq 0$ for all i, k, and matrices B^k are non-negative and irreducible for all k. Then, the healthy state is the unique equilibrium of (5) if and only if $s(B^k - D^k) \leq 0$ for all $k \in [m]$.*

Proof. Sufficiency has been shown in Lemma 2. Therefore, all that remains to be shown is that if for some $j \in [m]$, $s(B^j - D^j) > 0$, the system (5) admits an endemic state.

Without loss of generality, suppose $s(B^1 - D^1) > 0$. Set $p^k = \mathbf{0}$ for all $k = 2, \ldots, m$. Then, the dynamics of p^1 simplifies to a single-virus system, which admits an endemic state by Proposition 3 in Liu et al. (2019). Therefore, when $s(B^1 - D^1) > 0$, the system (5) always admits an equilibrium of the form $(\tilde{p}^1, \mathbf{0}, \ldots, \mathbf{0})$ with $\tilde{p}^1 \gg \mathbf{0}$. □

We next provide a result on global exponential stability for the case when the underlying subgraphs are undirected and the infection rates are symmetric.

Theorem 2. *Suppose B^k is symmetric, and the maximum eigenvalue of $B^k - D^k$ is less than zero, that is $\lambda_1(B^k - D^k) < 0$. Then, the healthy state is exponentially stable for virus k, with domain of attraction $\mathcal{D}$ in (6).*

Proof. Consider the Lyapunov function $V(p^k) = \frac{1}{2}(p^k)^T p^k$. For $p^k \neq \mathbf{0}$,

$$\begin{aligned}\dot{V}(p^k) &= (p^k)^T \dot{p}^k \\ &= (p^k)^T \left(B^k - \sum_{l=1}^{m} P^l B^k - D^k \right) p^k \\ &\leq (p^k)^T (B^k - D^k) p^k \\ &\leq \lambda_1(B^k - D^k) \|p^k\|^2 < 0.\end{aligned}$$

The first inequality holds as $(P^l B^k)_{ij} \geq 0, \ \forall l, i, j$ by construction, since each $p_i^l(t)$ is a probability. The second inequality holds by the Rayleigh–Ritz Theorem since $B^k - D^k$ is symmetric. Therefore, the system converges exponentially to the origin by Theorem 8.5 in Khalil (1996). □

3.2. Mutating dynamic graph case

We generalize the model from (4) to the dynamic graph case and allow the viruses to mutate over time giving

$$\dot{p}_i^k(t) = (1 - p_i^1(t) - \cdots - p_i^m(t)) \sum_{j=1}^{n} \beta_{ij}^k(t) p_j^k(t) - \delta_i^k(t) p_i^k(t), \quad (8)$$

where $\beta_{ij}^k(t)$ and $\delta_i^k(t)$ are functions of time and (8) holds for $k = 1, \ldots, m$. We now provide a sufficient condition for global exponential stability of the healthy state.

Theorem 3. *Suppose $B^k(t)$ is symmetric, $B^k(t) - D^k(t)$ is piecewise-continuous in t and bounded, and $\sup_{t\geq 0} \lambda_1(B^k(t) - D^k(t)) < 0$. Then, the healthy state is exponentially stable for virus k, with domain of attraction $\mathcal{D}$, as given in (6).*

Proof. Consider the Lyapunov function $V(p^k) = \frac{1}{2}(p^k)^T p^k$. For $p^k \neq \mathbf{0}$,

$$\begin{aligned}\dot{V}(p^k) &= (p^k)^T \dot{p}^k \\ &= (p^k)^T \left(B^k(t) - \sum_{l=1}^{m} P^l B^k(t) - D^k(t) \right) p^k \\ &\leq (p^k)^T (B^k(t) - D^k(t)) p^k \\ &\leq \lambda_1(B^k(t) - D^k(t)) \|p^k\|^2 \\ &\leq (\sup_{t\geq 0} \lambda_1(B^k(t) - D^k(t))) \|p^k\|^2 < 0.\end{aligned}$$

The first inequality holds since $(P^l B^k(t))_{ij} \geq 0, \ \forall l, i, j$ and $\forall t \geq 0$, by construction and Lemma 1. The second inequality holds by the Rayleigh–Ritz Theorem since $B^k(t) - D^k(t)$ is symmetric. The last inequality holds by definition of the supremum. Thus the system converges exponentially to the origin by Theorem 8.5 in Khalil (1996). □

Note that Theorem 3 is a generalization of Theorem 2, and Theorem 1 in Paré et al. (2015, 2018), and guarantees that if the healing rates dominate the infection rates coupled with the network structure, assuming symmetric infection graphs, then the viruses will be eradicated.

Under additional assumptions we can also show exponential stability for the case when infection rates are not symmetric and the underlying subgraphs are undirected.

Definition 1. For a given virus k, assume that for all $t \geq 0$, there exist $c^k(t), \lambda^k(t) > 0$ such that

$$\|B^k(t) - D^k(t)\| \leq c^k(t) e^{-\lambda^k(t) t} \quad \forall t \geq 0. \quad (9)$$

We then define

$$\gamma_1^k := \sup_{t\geq 0} \int_0^\infty c^k(t)^2 e^{-2\lambda^k(t)\tau} d\tau. \quad (10)$$

Note that

$$\gamma_1^k \geq \left\| \int_0^\infty e^{(B^k(t) - D^k(t))^T \tau} e^{(B^k(t) - D^k(t))\tau} d\tau \right\|, \quad (11)$$

which follows from the definition of γ_1^k and the upper bound assumption in (9).

Theorem 4. *Consider the dynamics for virus k in (8) with $B^k(t) - D^k(t)$ continuously differentiable and bounded, that is, there exists an $L > 0$ such that $\|B^k(t) - D^k(t)\| \leq L \ \forall t$. Assume $\sup_{t\geq 0} s(B^k(t) - D^k(t)) < 0$, and γ_1^k in Definition 1 is finite. If $\sup_{t>0} \|\dot{B}^k(t) - \dot{D}^k(t)\| < \frac{1}{2(\gamma_1^k)^2}$ or $\int_t^{t+T} \|\dot{B}^k(s) - \dot{D}^k(s)\| ds \leq \mu T + \alpha$ for small enough $\mu > 0$, then the healthy state is exponentially stable for virus k, with domain of attraction $\mathcal{D}$, as given in (6).*

Proof. Note that since $(P^l(t) B^k(t))_{ij} \geq 0 \ \forall l, i, j$, by construction,

$$\begin{aligned}\dot{p}^k &= (B^k(t) - \sum_{l=1}^{m} P^l B^k(t) - D^k(t)) p^k \\ &\leq (B^k(t) - D^k(t)) p^k.\end{aligned}$$

Therefore, by the Grönwall–Bellman Inequality (p. 651, Khalil, 1996), the solution of the original system will be bounded above by the solution of the linear system. Thus, by Lemma 2 in Paré et al. (2016), the healthy state is exponentially stable for virus k. □

Note that Theorem 4 is a generalization of a single-virus result provided in Paré et al. (2016, 2018), which is for a less general, non-mutating model; however the arguments for Lemma 2 in Paré et al. (2016) hold by replacing $BA(t)$ with $B^k(t)$, D with $D^k(t)$, and $B\dot{A}(t) - D$ with $\dot{B}^k(t) - \dot{D}^k(t)$. Theorem 4 states that if the linearized system is Hurwitz for all time, that is, the healing rates dominate the infection rates, and the virus does not mutate nor the graph change too quickly, then the virus is eradicated in exponential time.

Now we consider a case where the linearized system is not required to be always Hurwitz, that is, $s(B^k(t) - D^k(t)) < 0$ is not necessary for all $t > 0$, but only on the average. We also allow perturbations on the spread graph, denoted by $\Delta^k(t)$.

Theorem 5. *Consider the dynamics for single virus k:*

$$\dot{p}^k = (B^k(t) + \Delta^k(t) - \sum_{l=1}^{m} P^l (B^k(t) + \Delta^k(t)) - D^k(t)) p^k.$$

Assume for all $t_0 \geq 0$ that

$$\lim_{T\to\infty} \frac{1}{T} \int_{t_0}^{t_0+T} \|B^k(s) - D^k(s)\| ds \leq a < \infty, \quad (12)$$

and for some $\nu > 0$ there exists an $h > 0$ such that

$$\|B^k(t+h) - D^k(t+h) - (B^k(t) - D^k(t))\| \leq \nu h^\gamma, \quad (13)$$

for all $t \geq 0$ and some γ, $0 < \gamma \leq 1$. Assume further that

$$\lim_{T\to\infty} \frac{1}{T} \int_{t_0}^{t_0+T} s_1(B^k(s) - D^k(s))ds \leq \bar{\alpha} \tag{14}$$

for some negative scalar $\bar{\alpha}$ and for all $t_0 \geq 0$,

$$\lim_{T\to\infty} \frac{1}{T} \int_{t_0}^{t_0+T} \|\Delta^k(s)\|ds \leq \eta < \infty, \tag{15}$$

for all $t_0 \geq 0$, and for all i, j and $t \geq 0$, the perturbation satisfies the inequality

$$|\Delta_{ij}^k(t)| \leq \beta_{ij}^k(t). \tag{16}$$

Then, the origin is exponentially stable for virus k.

Proof. Since $(P^l(t)(B^k(t)+\Delta^k(t)))_{ij} \geq 0\ \forall i, j$ by (16) and Lemma 1,

$$\begin{aligned}\dot{p}^k &= (B^k(t) + \Delta^k(t) - \sum_{l=1}^{m} P^l(B^k(t) + \Delta^k(t)) - D^k(t))p^k \\ &\leq (B^k(t) + \Delta^k(t) - D^k(t))p^k.\end{aligned}$$

Therefore, by the Grönwall–Bellman Inequality the solution of the original system will be bounded above by the solution of the linear system. Thus, by Theorem 2 in Solo (1994), the origin is exponentially stable for virus k. □

This result says that if the linearized system is bounded on the average, slowly time-varying, Hurwitz on the average (but not necessarily strictly Hurwitz for all $t \geq 0$), that is, the healing rates do not need to always dominate the infection rates, and the perturbations are bounded and not too large, then the system converges to the healthy state. This fact is useful in control design; see Section 6.

4. Stability analysis of the endemic states

While virus eradication is the goal, it is not always attainable. Often viruses will persist and reach a nonzero equilibrium, which we call endemic states. In the following, similar to Section 3.1 we consider the non-mutating, static graph version of the system defined by the state equations given in (4). There are a number of different endemic equilibria for this system. The simplest scenario is when one virus is in an endemic state and the remaining viruses are eradicated.

Corollary 1. *Suppose that $\delta_i^k \geq 0$ for all i, k, and the matrices B^k are non-negative and irreducible for all k. If for some $i \in [m]$, $s(B^i - D^i) > 0$ and $s(B^k - D^k) \leq 0$ for all $k \neq i$, then (5) has two equilibria, the healthy state $(\mathbf{0}, \ldots, \mathbf{0})$, where the system converges to this equilibrium for all initial conditions in $\{(p^1, \ldots, p^m) | p^i = \mathbf{0}$ and $p^k \in [0, 1]^n\ \forall k \neq i\}$, and a unique endemic state of the form $(\mathbf{0}, \ldots, \mathbf{0}, \tilde{p}^i, \mathbf{0}, \ldots, \mathbf{0})$ with $\tilde{p}^i \gg \mathbf{0}$, which is asymptotically stable with domain of attraction $\mathcal{D} \setminus \{(p^1, \ldots, p^m) | p^i = \mathbf{0}$ and $p^k \in [0, 1]^n\ \forall k \neq i\}$, with $\mathcal{D}$ defined in (6).*

Note that the healthy state can be shown to be an unstable equilibrium by evaluating the Jacobian linearization at the origin. A small perturbation of virus i from the origin will drive the system to the unique endemic state.

Proof. From the proof of Lemma 2, $p^k(t)$ will asymptotically converge to $\mathbf{0}$ as $t \to \infty$ for all initial values $(p^1(0), \ldots p^m(0)) \in \{(p^1, \ldots, p^m) | p^i = \mathbf{0}$ and $p^k \in [0, 1]^n\ \forall k \neq i\}$, for $k \neq i$. From (5),

$$\dot{p}^i(t) = (B^i - D^i - P^i(t)B^i)p^i(t) - \sum_{k\neq i} P^k(t)B^k p^k(t).$$

Thus, we can regard the dynamics of $p^i(t)$ as an autonomous system

$$\dot{p}^i(t) = (B^i - D^i - P^i(t)B^i)p^i(t), \tag{17}$$

with a vanishing perturbation $-\sum_{k\neq i} P^k(t)B^i p^i(t)$, which converges to $\mathbf{0}$ as $t \to \infty$. From Proposition 3 in Liu et al. (2019), the autonomous system (17) will asymptotically converge to a unique endemic state $(\mathbf{0}, \ldots, \mathbf{0}, \tilde{p}^i, \mathbf{0}, \ldots, \mathbf{0})$ for any $(p^1(0), \ldots, p^m(0)) \in \mathcal{D} \setminus \{(p^1, \ldots, p^m) | p^i = \mathbf{0}$ and $p^k \in [0, 1]^n\ \forall k \neq i\}$, with $\mathcal{D}$ defined in (6).

Let $y(t) = p^i(t) - \tilde{p}^i$. Then $\dot{y}(t) = f(y(t)) + g(t, y(t))$, where

$$f(y(t)) = (-D^i + (I - \tilde{P}^i)B^i - \text{diag}(B^i p^i(t)))y(t)$$

$$g(t, y(t)) = -\sum_{k\neq i} P^k(t)B^i(y(t) + \tilde{p}^i).$$

Consider the Lyapunov function candidate

$$V(y(t)) = \max_{l\in[n]} \frac{|y_l(t)|}{\tilde{p}_l^i}.$$

Then,

$$\dot{V}(y(t)) = \frac{\partial V}{\partial y} f(y(t)) + \frac{\partial V}{\partial y} g(t, y(t)).$$

From the proof of Proposition 3 in Liu et al. (2019), $\frac{\partial V}{\partial t} + \frac{\partial V}{\partial y} f(t, y) < 0$ unless $y(t) = \mathbf{0}$, i.e., $x^i(t) = \tilde{x}^i$ (note Proposition 3 in Liu et al. (2019) is for the single virus case; we assert the obvious that if it is negative for one virus then additional viruses make it more negative). Since, $\forall k \neq i$, $p^k(t)$ asymptotically converges to $\mathbf{0}$, so does $\frac{\partial V}{\partial y} g(t, y(t))$. This implies that after a sufficiently long time, $\dot{V}(y(t)) < 0$ if $x^i(t)$ does not equal $\tilde{x}^i$. Using the same argument as in the proof of Proposition 3 in Liu et al. (2019), $(p^1(t), \ldots, p^m(t))$ will asymptotically converge to the unique endemic state $(\mathbf{0}, \ldots, \mathbf{0}, \tilde{p}^i, \mathbf{0}, \ldots, \mathbf{0})$ for any $(p^1(0), \ldots, p^m(0)) \in \mathcal{D} \setminus \{(p^1, \ldots, p^m) | p^i = \mathbf{0}$ and $p^k \in [0, 1]^n\ \forall k \neq i\}$, with $\mathcal{D}$ as in (6). □

Note that Corollary 1 states that if the healing parameters dominate the infection rates for all viruses except one, then only that one virus will survive. The result is a direct extension of Theorem 2 in Liu et al. (2019).

Another possible endemic state is that of coexisting equilibria, that is where more than one virus survives. To facilitate the next theorem that establishes this result, we rewrite the single virus model in (1) in matrix form:

$$\dot{z}(t) = (B^1 - Z(t)B^1 - D^1)z(t), \tag{18}$$

where z is the vector of p_i's and $Z = \text{diag}(z)$.

Theorem 6. *Suppose that $\delta_i^1 = \mu_2\delta_i^2 = \cdots = \mu_m\delta_i^m > 0$, $\forall i \in [n]$, $\beta_{ij}^1 = \mu_2\beta_{ij}^2 = \cdots = \mu_m\beta_{ij}^m\ \forall \beta_{ij}^k \neq 0$, $k \in [m]$, $\mu_k > 0\ \forall k \in [m]\setminus\{1\}$, the matrix B^1 is non-negative and irreducible, and $s(-D^1 + B^1) > 0$. We have that $(\tilde{p}^1, \ldots, \tilde{p}^m)$ with $\tilde{p}^k > \mathbf{0}\ \forall k \in [m]$ is an equilibrium of (4) if and only if $\tilde{p}^k \gg \mathbf{0}\ \forall k \in [m]$, $\tilde{p}^i = \alpha^{ik}\tilde{p}^k\ \forall i, k \in [m]$, for some constants $\alpha^{ik} > 0$, such that $\tilde{z} = \tilde{p}^1 + \cdots + \tilde{p}^m$, where $\tilde{z}$ is the nonzero endemic state of (18).*

Proof. From the assumption $\delta_i^1 = \mu_2\delta_i^2 = \cdots = \mu_m\delta_i^m > 0$, $\forall i \in [n]$ and $\beta_{ij}^1 = \mu_2\beta_{ij}^2 = \cdots = \mu_m\beta_{ij}^m\ \forall \beta_{ij}^k \neq 0$, $k \in [m]$ and $\mu_k > 0\ \forall k \in [m] \setminus \{1\}$, we have $B^1 = \mu_2 B^2 = \cdots = \mu_m B^m$ and $D^1 = \mu_2 D^2 = \cdots = \mu_m D^m$. These expressions, with (5), give

$$\mu_k\dot{p}^k(t) = (-D^1 + B^1 - (P^1(t) + \cdots + P^m(t))B^1)p^k(t) \tag{19}$$

for $k \in [m] \setminus \{1\}$. Thus, an equilibrium of $p^1(t) + \mu_2 p^2(t) + \cdots + \mu_m p^m(t)$ satisfies

$$[-D^1 + B^1 - ZB^1]z = \mathbf{0}, \tag{20}$$

where $z = p^1 + \cdots + p^m$, which is equivalent to the condition for an equilibrium of the single-virus model (18). From Proposition 2 of Liu et al. (2019) and the assumption $s(-D^1 + B^1) > 0$, $z(t)$ has a unique nonzero equilibrium in $[0, 1]^n$. Thus, $\tilde{z} = \tilde{p}^1 + \cdots + \tilde{p}^m$ is unique.

We will now show that $\tilde{p}^1 + \cdots + \tilde{p}^m \ll \mathbf{1}$. Suppose that, to the contrary, there exists an i such that $\tilde{p}_i^1 + \cdots + \tilde{p}_i^m = 1$. Therefore, there exists a $k \in [m]$ such that, by (4),

$$\dot{p}_i^k = -\delta_i^k \tilde{p}_i^k < 0,$$

by the assumption that $\delta_i^k > 0$. Thus, $\tilde{p}_i^1 + \cdots + \tilde{p}_i^m = 1$ is not an equilibrium, which is a contradiction. Therefore, $\tilde{p}^1 + \cdots + \tilde{p}^m \ll \mathbf{1}$. Thus, $-D^1 + (I - (\tilde{P}^1 + \cdots + \tilde{P}^m))B^1 = -D^1 + (I - \tilde{Z})B^1$ is an irreducible Metzler matrix. By Lemma 4 in Liu et al. (2019), since (20) holds and $p^1(t) + \cdots + p^2(t) \gg \mathbf{0}$, we have

$$s(-D^1 + B^1 - \tilde{Z}B^1) = 0 \tag{21}$$

with the corresponding eigenvector $\tilde{z} = \tilde{p}^1 + \cdots + \tilde{p}^m$.

From (5) and (19), the equilibria of $\dot{p}^1(t) - \mu_2 p^2(t) - \cdots - \dot{p}^m(t)$, …, $\dot{p}^1(t) + \cdots + \mu_{m-1}p^{m-1}(t) - \mu_m p^m(t)$ satisfy

$$\begin{aligned}
&(-D^1 + B^1 - \tilde{Z}B^1)(\tilde{p}^1 - \tilde{p}^2 - \cdots - \tilde{p}^m) = \mathbf{0},\\
&\qquad\qquad\vdots\\
&(-D^1 + B^1 - \tilde{Z}B^1)(\tilde{p}^1 + \cdots + \tilde{p}^{m-1} - \tilde{p}^m) = \mathbf{0}.
\end{aligned} \tag{22}$$

From Lemma 3 in Liu et al. (2019), the eigenvector corresponding to $s(-D + B - \tilde{Z}B)$ is unique up to a constant and is strictly greater than zero. Therefore, by (21), either

$$\begin{aligned}
\tilde{p}^1 + \cdots + \tilde{p}^m &= \gamma_1(\tilde{p}^1 + \cdots + \tilde{p}^{m-1} - \tilde{p}^m)\\
&\vdots\\
&= \gamma_{m-1}(\tilde{p}^1 - \tilde{p}^2 - \cdots - \tilde{p}^m),
\end{aligned} \tag{23}$$

for some constants $\gamma_i > 0$, or the vectors are all equal to $\mathbf{0}$. Without loss of generality, if the first equation of (22) has the vector equal to $\mathbf{0}$, then $\tilde{p}^1 = \tilde{p}^2 + \cdots + \tilde{p}^m$. Using these expressions and/or the expressions from (23), for any i, $\tilde{p}^i = \alpha^{ik}\tilde{p}^k$ for some constant $\alpha^{ik} > 0$, and thus $\tilde{p}^1, \ldots, \tilde{p}^m \gg \mathbf{0}$. This completes the sufficiency proof.

Now, for necessity, assume there exist $\tilde{p}^k \gg \mathbf{0}\ \forall k \in [m]$, where $\tilde{p}^i = \alpha^{ik}\tilde{p}^k\ \forall i, k \in [m]$, for some constants $\alpha^{ik} > 0$, such that $\tilde{z} = \tilde{p}^1 + \cdots + \tilde{p}^m$, where $\tilde{z}$ is the nonzero endemic state of (18). Since $\tilde{z} = \tilde{p}^1 + \cdots + \tilde{p}^m$ is an equilibrium of (18), (20) holds. By the assumption that $\tilde{p}^i = \alpha^{ik}\tilde{p}^k\ \forall i, k \in [m]$, $\tilde{z} = (1 + \sum_{i \neq k} \alpha^{ik})\tilde{p}^k$. Since $\tilde{p}^k \gg \mathbf{0}\ \forall k \in [m]$ and from Lemma 3 in Liu et al. (2019) we know that $\tilde{z}$ is unique up to a scalar, we have, for each $k \in [m]$,

$$[-D^1 + B^1 - ZB^1]\tilde{p}^k = \mathbf{0}.$$

Therefore, from (19), we have that $(\tilde{p}^1, \ldots, \tilde{p}^m)$ is an equilibrium of (4). □

We can now state the following two corollaries of Theorem 6, which are non-trivial extensions (necessity is added) of Theorems 6 and 7 in Liu et al. (2019), respectively.

Corollary 2. *Consider the model in (4) with each virus propagating over the same strongly connected graph $\mathbb{G}$ with corresponding adjacency matrix A, and each virus homogeneous in healing and infection rates, that is, for each $k \in [m]$ $\delta_i^k = \delta^k > 0\ \forall i \in [n]$ and $\beta_i^k = \beta^k > 0\ \forall i \in [n]$. Suppose $s(A) > \frac{\delta^1}{\beta^1} = \cdots = \frac{\delta^m}{\beta^m}$. We then have $(\tilde{p}^1, \ldots, \tilde{p}^m)$ with $\tilde{p}^k > \mathbf{0}\ \forall k \in [m]$ is an equilibrium of (4) if and only if $\tilde{p}^k \gg \mathbf{0}\ \forall k \in [m]$, $\tilde{p}^i = \alpha^{ik}\tilde{p}^k\ \forall i, k \in [m]$, for some constants $\alpha^{ik} > 0$, such that $\tilde{z} = \tilde{p}^1 + \cdots + \tilde{p}^m$, where $\tilde{z}$ is the nonzero endemic state of (18).*

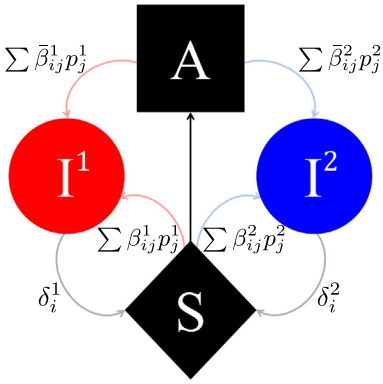

Fig. 2. Two competing viruses with an awareness state. The label on the black arrow is $\sum_{j=1}^{n} \kappa_{ij} \sum_{k=1}^{m} p_j^k + \sum_{j=1}^{n} \bar{\kappa}_{ij} y_j$.

Corollary 3. *Suppose that $\delta_i^1 = \cdots = \delta_i^m > 0$, $\forall i \in [n]$ (which implies that $D^1 = \cdots = D^m = D$), $\beta_{ij}^1 = \cdots = \beta_{ij}^m\ \forall \beta_{ij}^k \neq 0$, $k \in [m]$ (which implies that $B^1 = \cdots = B^m = B$), the matrix B is nonnegative and irreducible, and $s(-D + B) > 0$. We then have that $(\tilde{p}^1, \ldots, \tilde{p}^m)$ with $\tilde{p}^k > \mathbf{0}\ \forall k \in [m]$ is an equilibrium of (4) if and only if $\tilde{p}^k \gg \mathbf{0}\ \forall k \in [m]$, $\tilde{p}^i = \alpha^{ik}\tilde{p}^k\ \forall i, k \in [m]$, for some constants $\alpha^{ik} > 0$, such that $\tilde{z} = \tilde{p}^1 + \cdots + \tilde{p}^m$, where $\tilde{z}$ is the nonzero endemic state of (18).*

While stability of the time-varying case has been explored in Paré et al. (2018), the existence of an endemic limit cycle is an open problem, even for the single-virus case. Sufficient conditions for the existence of a periodic endemic cycle for a single-virus switching system are provided in Rami et al. (2014).

5. Human awareness

As has been seen with COVID-19, when agents become aware of viral spread in their vicinity, their behaviors change (Lewnard & Lo, 2020). We extend the model in (4) to allow agents to become alerted when viruses are pervading the system, as in Fig. 2. Such awareness reduces the likelihood of becoming infected, by scaling the spread parameters. We introduce $y_i(t)$ to denote the portion of alert individuals in group i. Thus, for every $k \in [m]$,

$$\begin{aligned}
\dot{p}_i^k(t) = &\left(1 - p_i^1(t) - \cdots - p_i^m(t) - y_i(t)\right) \sum_{j=1}^{n} \beta_{ij}^1 p_j^k(t)\\
&- \delta_i^k p_i^k(t) + y_i(t) \sum_{j=1}^{n} \bar{\beta}_{ij}^k p_j^k(t),
\end{aligned} \tag{24}$$

$$\begin{aligned}
\dot{y}_i(t) = &-\mu_i y_i(t) - y_i(t) \sum_{k=1}^{m} \sum_{j=1}^{n} \bar{\beta}_{ij}^k p_j^k(t)\\
&+ (1 - p_i^1(t) - \cdots - p_i^m(t) - y_i(t)) \sum_{j=1}^{n} \kappa_{ij} \sum_{k=1}^{m} p_j^k(t)\\
&+ (1 - p_i^1(t) - \cdots - p_i^m(t) - y_i(t)) \sum_{j=1}^{n} \bar{\kappa}_{ij} y_j(t),
\end{aligned} \tag{25}$$

where μ_i is the death rate, κ_{ij} are the alerting rates from infected neighbors, $\bar{\kappa}_{ij}$ are the alerting rates from alerted neighbors, and $\bar{\beta}_{ij}^1$ and $\bar{\beta}_{ij}^2$ are the infection rates associated with the alert state, with $\bar{\beta}_{ij}^1 < \beta_{ij}^1$ and $\bar{\beta}_{ij}^2 < \beta_{ij}^2$ for all $i, j \in [n]$. Note that κ_{ij} allows for awareness from infected individuals and $\bar{\kappa}_{ij}$ allows for

awareness from individuals who are already aware. We define K and $\bar{K}$ as the matrices of κ_{ij}'s and $\bar{\kappa}_{ij}$'s, respectively. The model in (25) can be derived in a manner similar to that in Section 2, following (Liu et al., 2017), and is still well defined, as illustrated by the following lemma.

Lemma 3. *Suppose that for all $i \in [n], k \in [m]$, we have $\delta_i^k \geq 0$, $\mu_i \geq 0$, and the matrices B^k, $\bar{B}^k$, K, $\bar{K}$ are non-negative. If for all $i \in [n], k \in [m]$, we have $p_i^k(0), y_i(0), (1 - p_i^1(0) - \cdots - p_i^m(0) - y_i(0)) \in [0, 1]$, then $p_i^k(t), y_i(t), p_i^1(t) + \cdots + p_i^m(t) + y_i(t) \in [0, 1]$ for all $i \in [n], k \in [m]$ and $t \geq 0$.*

The proof follows the lines similar to those of Lemma 1.

Following the definitions in Liu et al. (2017), an equilibrium $(p^1, \ldots, p^m, y)$ of (24)–(25) is a *healthy state* if $p^1 = \cdots = p^m = \mathbf{0}$, independent of the value of y, since at such an equilibrium, all individuals in the network are healthy. We call the equilibrium where $p^1 = \cdots = p^m = y = \mathbf{0}$ the trivial healthy state. If a healthy state has $y > \mathbf{0}$, it is an *alert state*, which implies that all individuals are healthy, but some of them are alert. Similar to the multi-virus model, the system with human awareness also admits *endemic states* which are equilibria with nonzero p^k's, which will be illustrated via simulations in Section 7. The following theorem provides a sufficient condition for global stability of healthy states.

Theorem 7. *Suppose that for all $i \in [n], k \in [m]$, we have $\delta_i^k \geq 0$ and the matrices B^k, $\bar{B}^k$ are non-negative and irreducible. If $s(B^k - D^k) \leq 0$ for all $k \in [m]$, then the system in (24)–(25) asymptotically enters the set of healthy states. Suppose, in addition, that $\bar{K}$ is irreducible. If $s(-M + \bar{K}) \leq 0$, then the system in (24)–(25) has a unique equilibrium $(\mathbf{0}, \ldots, \mathbf{0})$, which is asymptotically stable with domain of attraction $\mathcal{D}$ defined in (6). If $s(-M + \bar{K}) > 0$, then the system in (24)–(25) has two equilibria, the trivial healthy state $(\mathbf{0}, \ldots, \mathbf{0})$, which is asymptotically stable with domain of attraction $\{(p^1, \ldots, p^m, \mathbf{0}) | p^1 \geq \mathbf{0}, \ldots, p^m \geq \mathbf{0}, p^1 + \cdots + p^m \leq \mathbf{1}\}$, and a unique alert state $(\mathbf{0}, \ldots, \mathbf{0}, \tilde{y})$ with $\tilde{y} \gg \mathbf{0}$, which is asymptotically stable with domain of attraction $\mathcal{D} \setminus \{(p^1, \ldots, p^m, \mathbf{0}) | p^1 \geq \mathbf{0}, \ldots, p^m \geq \mathbf{0}, p^1 + \cdots + p^m \leq \mathbf{1}\}$.*

Proof. Since $p_i^1(t), \ldots, p_i^m(t)$, and $y_i(t)$ are always nonnegative by Lemma 3, from (24)–(25), we have for every $k \in [m]$, $\dot{p}_i^k(t) \leq -\delta_i^k p_i^k(t) + (1 - p_i^k(t)) \sum_{j=1}^n \beta_{ij}^k p_j^k(t)$, which implies that each of the trajectories of each $p_i^k(t)$ is bounded above by a single-virus model. Therefore, if $s(-D^k + B^k) \leq 0$ for every virus $k \in [m]$, $p_i^k(t)$ will asymptotically converge to $\mathbf{0}$ as $t \to \infty$, for every virus $k \in [m]$, and thus the system asymptotically enters the set of healthy states.

Next suppose that $\bar{K}$ is irreducible. From (25), we have

$$\begin{aligned}\dot{y}(t) = & -My(t) - Y(t) \sum_{k=1}^m \bar{B}^k p^k(t) \\ & + (I - P^1(t) - \cdots - P^m(t) - Y(t))K \times \\ & (p^1(t) + \cdots + p^m(t)) \\ & + (I - P^1(t) - \cdots - P^m(t) - Y(t))\bar{K}y(t).\end{aligned}$$

Thus, we can regard the dynamics of $y(t)$ as an autonomous system,

$$\dot{y}(t) = (\bar{K} - Y(t)\bar{K} - M)y(t),$$

with a vanishing perturbation $-Y(t) \sum_{j=1}^n \beta_{ij}^1 p_j^k(t) + (I - P^1(t) - \cdots - P^m(t) - Y(t))K(p^1(t) + \cdots + p^m(t)) - (P^1(t) + \cdots + P^m(t))\bar{K}y(t)$, which converges to $\mathbf{0}$ as $t \to \infty$ since all $p^1(t), \ldots, p^m(t)$ converge to $\mathbf{0}$. From Propositions 3 and 5 in Liu et al. (2016), it can be verified that $y(t)$ will asymptotically converge to $\mathbf{0}$ for any $y(0) \in [0, 1]^n$ if $s(-M + \bar{K}) \leq 0$, or a unique nonzero state $\tilde{y} \gg \mathbf{0}$ for any $y(0) \in [0, 1]^n \setminus \{\mathbf{0}\}$ if $s(-M + \bar{K}) > 0$. Therefore, if $s(-M + \bar{K}) \leq 0$, system (5) has a unique equilibrium $(\mathbf{0}, \ldots, \mathbf{0})$, which is asymptotically stable with domain of attraction $\mathcal{D}$, and if $s(-M + \bar{K}) > 0$, system (5) has a unique alert state $(\mathbf{0}, \ldots, \mathbf{0}, \tilde{y})$ with $\tilde{y} \gg \mathbf{0}$, which is asymptotically stable with domain of attraction $\mathcal{D} \setminus \{(p^1, \ldots, p^m, \mathbf{0}) | p^1 \geq \mathbf{0}, \ldots, p^m \geq \mathbf{0}, p^1 + \cdots + p^m \leq \mathbf{1}\}$, and $(\mathbf{0}, \ldots, \mathbf{0})$ is asymptotically stable with domain of attraction $\{(p^1, \ldots, p^m, \mathbf{0}) | p^1 \geq \mathbf{0}, \ldots, p^m \geq \mathbf{0}, p^1 + \cdots + p^m \leq \mathbf{1}\}$. □

Theorem 7 provides conditions for eradication of all the viruses, and the agents either return to a normal state or remain in an alert state. The alert equilibrium can be interpreted as the outbreak permanently changing people's behavior even after eradication.

6. Antidote control formulation

In this section, using the results from the preceding sections we develop mitigation strategies that minimize the impact of outbreaks. Let us assume that for each agent, or group (depending on the model interpretation), there is a control input $u_i(t)$ that acts as an additive boost to the healing rate. This implies that the controller can increase the ability of the agents, or groups, to recover from the virus, which can be thought of as administration of an antidote or some other type of treatment. This effect is portrayed in the model as

$$\dot{p}_i^k(t) = (1 - p_i^1(t) - \cdots - p_i^m(t)) \sum_{j=1}^n \beta_{ij}^k p_j^k(t) - (\delta_i^k(t) + u_i^k(t))p_i^k(t).$$

We define $U(t) = \text{diag}(u)$ with $u = [u_1(t), \ldots, u_n(t)]^T$. To simplify the discussion in this section, we assume $B^k(t) - D^k(t)$ is piecewise continuous in t and bounded $\forall t \geq 0$. Similar to the approaches in Pasqualetti et al. (2014), Preciado et al. (2014), Vijayshankar and Roy (2012) and Wan et al. (2007, 2008), we focus on minimizing the maximum eigenvalue of $B^k(t) - (D^k(t) + U^k(t))$. Even though these control techniques are generally effective, we believe the approaches herein are more general and simpler, and therefore more scalable. The assumption that our control input is additive to the base healing rate is novel and more sensible for the motivating examples, that is, every agent, or group, has some underlying inherent healing rate that should not be reduced by the controller.

While the solutions to the following posed problems may not meet the conditions of Lemma 2 and Theorem 4, that is, they may not result in the maximum real part of the eigenvalues always being less than zero, they push the system toward those conditions, consistent with the principle of the time-average being less than zero, presented in Theorem 5. And in practice, illustrated by simulations in the next section, these techniques reduce the spread of the epidemics. For static graphs/non-mutating viruses, these programs only need to be solved once, but if the system parameters (graph structure and/or spread parameters) change as a function of time, then the programs should be solved at a rate, preferably, that is faster than the change in the graph/spread parameters. Under the aforementioned assumptions we can formulate the following optimization problem for each virus k:

$$\begin{aligned}\underset{u_i^k(t)}{\textit{minimize}} \quad & s(B^k(t) - (D^k(t) + U^k(t))) \\ \textit{subject to} \quad & \sum_{i=1}^n u_i^k(t) \leq c^k, \quad t \geq 0, \\ & U^k(t) = \text{diag}(u_1^k(t), \ldots, u_n^k(t)), \\ & u_i^k(t) \geq 0, \quad i = 1, \ldots, n, \ t \geq 0.\end{aligned}$$

From the Gershgorin Disk Theorem (Horn & Johnson, 2012, p. 344) it is clear that by sufficiently increasing the u_i^k's, the conditions of Lemma 2 and Theorems 4 will be satisfied. Thus, we can relax the above optimization problem to the following:

Problem 1. For each virus $k \in [m]$,

$$\begin{aligned} \underset{\eta^k, u_i^k(t)}{\text{minimize}} \quad & \eta^k \\ \textit{subject to} \quad & \eta^k \geq \sum_{j=1}^{n} \beta_{ij}^k(t) - (\delta_i^k(t) + u_i^k(t)),\ i = 1, \ldots, n, \\ & \sum_{i=1}^{n} u_i^k(t) \leq c^k, \\ & u_i^k(t) \geq 0, \quad i = 1, \ldots, n,\ t \geq 0. \end{aligned}$$

This is clearly a linear program and can easily be solved.

To make this a more compelling and realistic problem, we can impose a constraint on the number of agents, or groups, that can be affected, which is a reasonable assumption because the cost of providing a low-dose treatment to all agents, or groups, is higher than that of providing that same amount of total treatment divided among a few select members of the population (such as the most infectious or most susceptible agents, or groups).

Employing the sparsity metric, $\|\cdot\|_0$, defined as the number of the non-zero entries in its argument, results in the following problem, with a capacity constraint and a sparsity constraint for each virus $k \in [m]$:

$$\begin{aligned} \underset{\eta^k, u_i^k(t)}{\textit{minimize}} \quad & \eta^k \\ \textit{subject to} \quad & \eta^k \geq \sum_{j=1}^{n} \beta_{ij}^k(t) - (\delta_i^k(t) + u_i^k(t)),\ i = 1, \ldots, n, \\ & \sum_{i=1}^{n} u_i^k(t) \leq c^k, \\ & \|u^k(t)\|_0 \leq d^k, \\ & u_i^k(t) \geq 0, \quad i = 1, \ldots, n,\ t \geq 0, \end{aligned}$$

where d^k is the maximum number of agents, or groups, that can be treated for virus k. At first glance, the second and third constraints may seem redundant; however, the ℓ_1 constraint limits the total amount of antidote that can be used while the sparsity constraint limits the number of agents, or groups, that can be treated. The inclusion of the ℓ_1 constraint prevents assigning an amount of antidote greater than that available for administration to the limited number of agents, or groups, allowed by the sparsity constraint.

It is well known that $\|\cdot\|_0$ is highly non-convex (Wright et al., 2009), making the above problem difficult to solve. Therefore, we employ a relaxation using the reweighted ℓ_1 norm (Candes et al., 2008).

Definition 2. The weighted ℓ_1 norm is

$$\|x^k\|_{\hat{\ell}_1} := \sum_{i=1}^{n} w_i^k |x_i^k|, \tag{26}$$

with $w_i > 0$, which can be a constant or depend on time.

In view of Definition 2, we can rewrite the above problem with the sparsity metric as the following:

ATA Algorithm:

$w^0 = vec(\frac{1}{n}, \ldots, \frac{1}{n})$
$k = 1$
While $\|u_k - u_{k-1}\| > \varepsilon$:
  $u_k = \arg\min$ **Problem 2**(w_{k-1})
  $w_i^k = \frac{1}{|u_i^k| + \epsilon}$
  $k = k + 1$

Fig. 3. ATA Algorithm.

Problem 2. For each virus $k \in [m]$,

$$\begin{aligned} \underset{\eta^k, u_i^k(t)}{\text{minimize}} \quad & \eta^k + \kappa \|u^k(t)\|_{\hat{\ell}_1} \\ \text{subject to} \quad & \eta^k \geq \sum_{j=1}^{n} \beta_{ij}^k(t) - (\delta_i^k(t) + u_i^k(t)),\ i = 1, \ldots, n, \\ & \sum_{i=1}^{n} u_i^k(t) \leq c^k, \\ & u_i^k(t) \geq 0, \quad i = 1, \ldots, n,\ t \geq 0, \end{aligned}$$

where κ is a constant weighting factor.

There are various heuristics for solving the reweighted ℓ_1 minimization problem (Candes et al., 2008; Daubechies et al., 2010; Lai et al., 2013); we employ the process for the selection of the weights w_i^k's in (26) proposed in Candes et al. (2008), which is, for some small $\epsilon > 0$,

$$w_i^{k+1} = \frac{1}{|x_i^k| + \epsilon}. \tag{27}$$

For completeness, we include the Antidote Treatment Administration (ATA) Algorithm in Fig. 3, which explains the implementation of this heuristic to solve Problem 2. The notation Problem 2(w_{k-1}) indicates that w_{k-1} is used for the weighted ℓ_1 norm in the objective function of Problem 2 in the kth iteration. Employing this heuristic yields a good solution to Problem 2 but clearly is computationally expensive, since it requires the calculation of multiple solutions. The effectiveness of this approach is illustrated in the following section via simulation.

7. Simulations

In this section, we present a set of simulations of various competing virus models over static and time-varying graph structure networks. Due to the difficulty in adequately displaying multiple viruses over networks of high dimensions, for the simulations we employ only three competing viruses, $m = 3$. Virus 1 is depicted by the color red (r), virus 2 is depicted by the color blue (b), and virus 3 is depicted by the color green (g). For all $i \in [n]$, the color at each time t for node i is given by

$$\frac{p_i^1(t)}{\sum_{k=1}^{3} p_i^k(t)} r + \frac{p_i^2(t)}{\sum_{k=1}^{3} p_i^k(t)} b + \frac{p_i^3(t)}{\sum_{k=1}^{3} p_i^k(t)} g. \tag{28}$$

When $p_i^1(t) + p_i^2(t) + p_i^3(t) = 0$, the color is black, which indicates completely healthy/susceptible. These color variations are used to facilitate the depiction of the parallel equilibrium ($\tilde{p}^1 = \alpha^2 \tilde{p}^2 = \alpha^3 \tilde{p}^3$), which are illustrated by all the nodes converging to the same color. For all $i \in [n]$, the diameter of node i is given by

$$d_0 + (p_i^1(t) + p_i^2(t) + p_i^3(t)) r_0, \tag{29}$$

with d_0 being the default/smallest diameter and r_0 being the scaling factor depending on the total combined infection level of

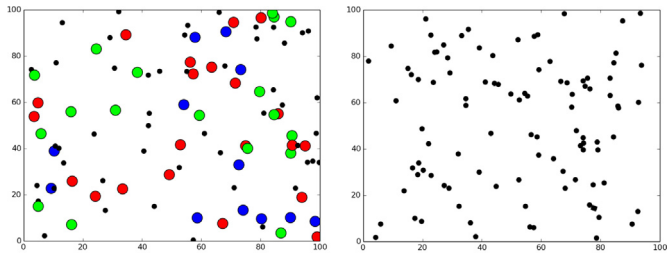

(a) Initial system condition. (b) The system at t=1000.

Fig. 4. Viruses 1 and 2 of this three-virus system meet the assumptions of Theorem 3 and so converge quickly to the healthy state, as does the third virus eventually. The colors and diameters follow (28) and (29) and the graph structure follows (30)–(32). A video of this simulation can be found at youtu.be/j_MHm08dA_o. (For interpretation of the references to color in this figure legend, the reader is referred to the web version of this article.)

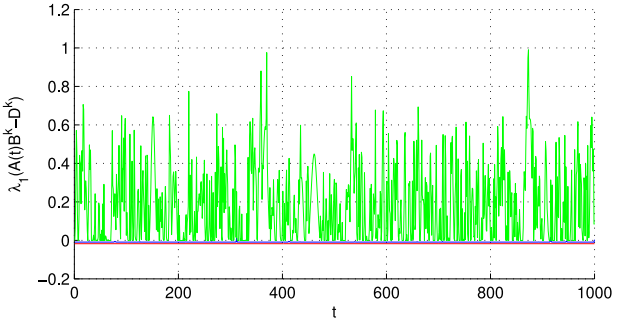

Fig. 5. The maximum eigenvalues of the three viruses from the simulation in Fig. 4. Note that the maximum eigenvalues for viruses 1 and 2 are indicated by horizontal lines (red and blue, resp.) just below the 0 axis, and maximum eigenvalues of virus 3 are given by the green line. (For interpretation of the references to color in this figure legend, the reader is referred to the web version of this article.)

node i. Therefore, the color indicates the type of virus(es) each agent/group has and the diameter indicates degree of infection for each agent/group.

For systems with three different subgraphs, viruses 1, 2, and 3 spread over graphs depicted by gray, green, and pink edges, respectively. If all viruses spread on the same graph, the edges are gray.

The simulation in Fig. 4 has three viruses spreading over the same time-varying graph. Similar to Paré et al. (2018), the graph structure is determined by

$$\beta_{ij}(t) = \begin{cases} \beta e^{-\|z_i(t)-z_j(t)\|^2}, & \text{if } \|z_i(t)-z_j(t)\| < \hat{r}, \\ 0, & \text{otherwise}, \end{cases} \tag{30}$$

where $z_i(t) \in \mathbb{R}^2$ is the position of node i, with $\hat{r} = 10$. The nodes have piece-wise constant drifts, that is,

$$\dot{z}(t) = \phi(t), \tag{31}$$

where $\phi(t) \in \mathbb{R}^2$ and is determined, for each dimension $l \in [2]$, by

$$\phi_l = \begin{cases} -\phi_l, & \text{if } z_l = z_{c_l} + \gamma/2 \text{ or } z_l = z_{c_l} - \gamma/2, \\ \phi_l, & \text{otherwise}, \end{cases} \tag{32}$$

and the nodes hover around a square, centered at some point z_c. The initial positions and ϕ's are chosen randomly. Each virus is homogeneous in infection rate. The first two viruses meet the assumptions of Theorem 3, while the maximum eigenvalue of the third virus fluctuates between being positive and negative. See Fig. 5 for a plot of the maximum eigenvalues of the three-virus

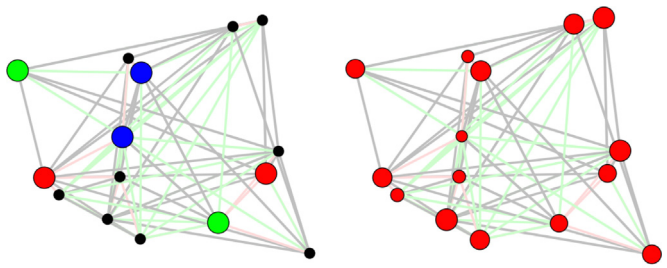

(a) Initial system condition. (b) The system at t=300.

Fig. 6. This three-virus system meets the assumptions of Corollary 1 so virus 1 reaches an endemic state while the other viruses are eradicated. The colors and diameters follow (28) and (29). A video of this simulation can be found at youtu.be/gPGwAdLo_DU. (For interpretation of the references to color in this figure legend, the reader is referred to the web version of this article.)

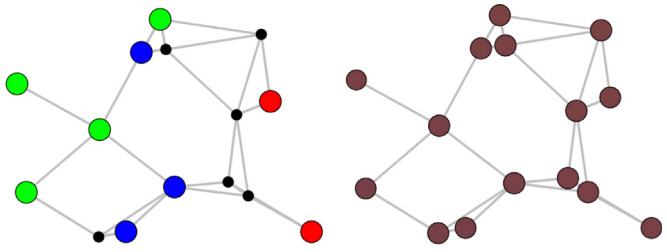

(a) Initial system condition. (b) The system at t=150.

Fig. 7. This three-virus system meets the assumptions of Corollary 2 and the viruses converge to a parallel equilibrium. The colors and diameters follow (28) and (29). A video of this simulation can be found at youtu.be/yzV8HxDkEJc. (For interpretation of the references to color in this figure legend, the reader is referred to the web version of this article.)

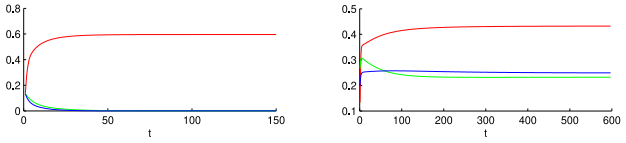

(a) Averages for Figure 6. (b) Averages for Figure 7.

Fig. 8. Average infections for Figs. 6 and 7.

dynamics. Consistent with Theorem 3 the first two viruses are eradicated quickly; the third virus takes longer to eliminate. This is illustrated in Fig. 4(b) by all the nodes being black.

The simulation shown in Fig. 6 meets the assumptions of Corollary 1, where $s(B^1 - D^1) > 0$, $s(B^2 - D^2) < 0$ and $s(B^3 - D^3) < 0$. Therefore, the first virus, depicted in red, reaches an endemic equilibrium, while the other two viruses are eradicated. The average infection values over time are shown in Fig. 8(a).

The simulation shown in Fig. 7 meets the assumptions of Corollary 2, that is, the three viruses are each homogeneous with $\frac{\delta^1}{\beta^1} = \frac{\delta^2}{\beta^2} = \frac{\delta^3}{\beta^3}$, and propagate over the same graph structure. There are 15 nodes with initial conditions given in Fig. 7(a). Consistent with the corollary, the dynamics of the system converge to a co-existing parallel equilibrium, depicted in Fig. 7(b) by the nodes being all the same color.

Similarly, the simulation shown in Fig. 9 meets the assumptions of Corollary 3, that is, the viruses are heterogeneous but identical for each node, with $\delta_i^1 = \cdots = \delta_i^m$, $\beta_i^1 = \cdots = \beta_i^m$ $\forall i \in [n]$, and propagate over the same graph structure. There are 15 nodes with initial conditions given in Fig. 9(a). Consistent

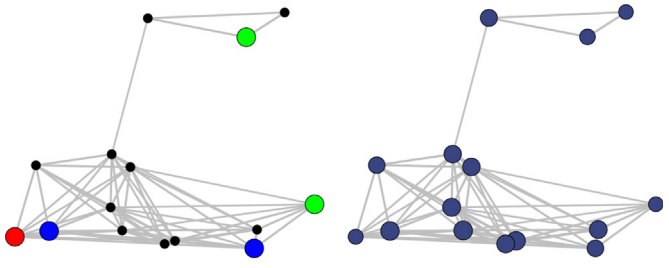

(a) Initial system condition. (b) The system at t=150.

Fig. 9. This three-virus system meets the assumptions of Corollary 3 and the viruses converge to a parallel equilibrium. The colors and diameters follow (28) and (29). A video of this simulation can be found at youtu.be/VIgoHe74P1w. (For interpretation of the references to color in this figure legend, the reader is referred to the web version of this article.)

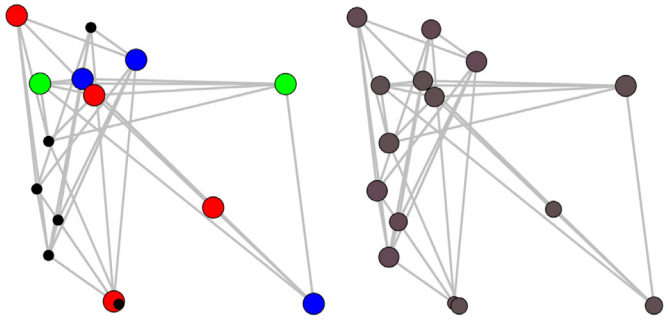

(a) Initial system condition. (b) The system at t=500.

Fig. 10. This three-virus system meets the assumptions of Theorem 6 and the viruses converge to a parallel equilibrium. The colors and diameters follow (28) and (29). A video of this simulation can be found at youtu.be/nyCl5FfRrZQ. (For interpretation of the references to color in this figure legend, the reader is referred to the web version of this article.)

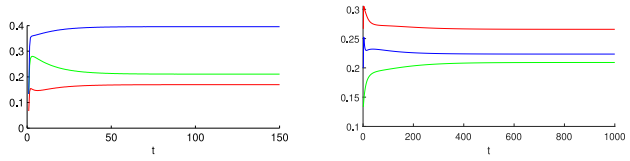

(a) Averages for Figure 9. (b) Averages for Figure 10.

Fig. 11. Average infections for Figs. 9 and 10.

with the corollary, the dynamics of the system converge to a co-existing parallel equilibrium, as shown in Fig. 9(b) by the nodes being all the same color.

We now consider a system that meets the assumptions of Theorem 6, that is, the three viruses are heterogeneous and $B^1 = 2B^2 = 0.5B^3$ and $D^1 = 2D^2 = 0.5D^3$. There are 15 nodes with initial conditions given in Fig. 10(a). Consistent with the theorem, the dynamics of the system converge to a co-existing parallel equilibrium, as shown in Fig. 10(b) by the nodes being all the same color.

Next, we illustrate the coupling of the multi-virus model with human awareness, as expounded upon in Section 5. To illustrate these results, we shift from circle nodes to polygons. The awareness variable is depicted by the rotation of the polygon, with the

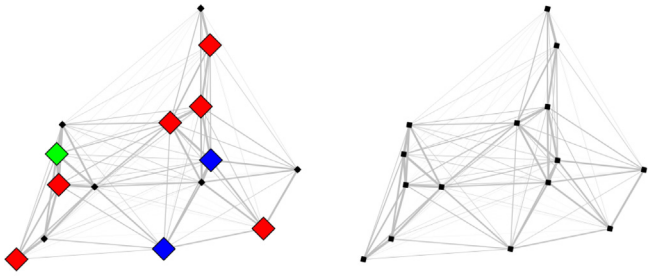

(a) Initial system condition. (b) The system at t=500.

Fig. 12. This three-virus system meets the assumptions of Theorem 7 with $s(-M+\bar{K}) > 0$ and the dynamics of the system converge to an alert state. The colors, sizes, and oreintations follow (28), (29) and (33). A video of this simulation can be found at youtu.be/Hq63uXpmjjM. (For interpretation of the references to color in this figure legend, the reader is referred to the web version of this article.)

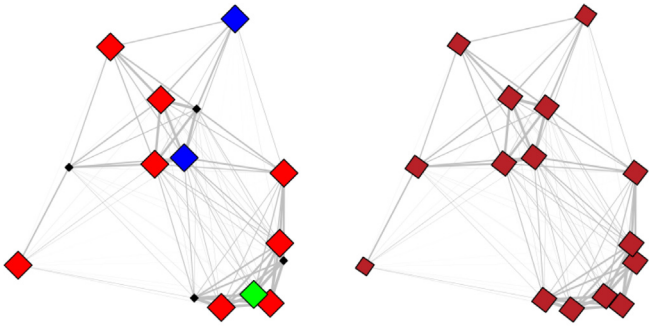

(a) Initial system condition. (b) The system at t=500.

Fig. 13. This three-virus system does not meet the assumptions of Theorem 7 and the dynamics of the system converge to an alert, parallel endemic state. The colors, sizes, and oreintations follow (28), (29) and (33). A video of this simulation can be found at youtu.be/dXnjSJQa4Qo. (For interpretation of the references to color in this figure legend, the reader is referred to the web version of this article.)

awareness state corresponding to different angles:

$$\begin{aligned} y_i = 0 &: \text{ diamond orientation,} \\ y_i = 1 &: \text{ square orientation,} \end{aligned} \tag{33}$$

and, for values in between, the orientation is linearly interpolated between the two. The coloring and size schemes remain the same. We consider a system that meets the assumptions of Theorem 7, that is, $s(B^k - D^k) \leq 0$ for all $k \in [3]$ and $s(-M+\bar{K}) > 0$. Consistent with the theorem, the dynamics of the system converge to an alert state, where the viruses vanish but the nodes remain alert, as shown in Fig. 12(b), by the black nodes (healthy) with rotated polygons (alert), and Fig. 14(a), by the average level of the viruses going to zero but the average awareness level converging to a nonzero value.

In Fig. 13, we depict a system where $s(B^k - D^k) > 0$ for all $k \in [3]$ and $s(-M+\bar{K}) > 0$. As expected, this system converges to an endemic state. It is worth noting that the system here was designed to meet the assumptions in Corollary 2, that is, the three viruses are homogeneous, with $\frac{\delta^1}{\beta^1} = \frac{\delta^2}{\beta^2} = \frac{\delta^3}{\beta^3}$, and the system converges to a parallel equilibrium similarly, even when awareness is included, depicted in Fig. 13(b) by the nodes being all the same color. The average infection values over time are shown in Fig. 14(b).

We conclude with implementations of the control techniques presented in Section 6. Consider the single-virus system in Fig. 15.

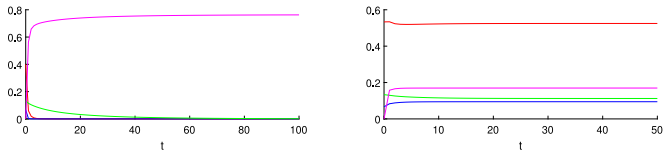

(a) Averages for Figure 12. (b) Averages for Figure 13.

Fig. 14. Average infections for Figs. 12 and 13. Magenta depicts the average awareness level. (For interpretation of the references to color in this figure legend, the reader is referred to the web version of this article.)

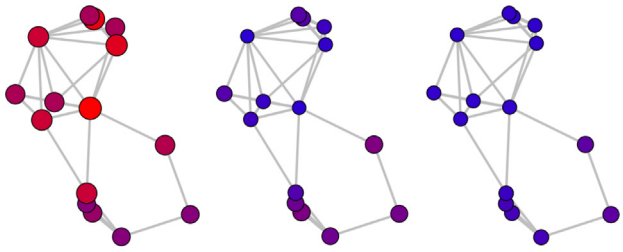

(a) No control (b) Using Prob. 1 (c) Using Prob. 2

Fig. 15. This is a single-virus (therefore blue indicates healthy here) endemic equilibrium comparing control techniques, depicting the final states with no control, using Problem 1, and implementing Algorithm 3 on Problem 2. A video of this simulation can be found at youtu.be/MhW95R8s_Po. (For interpretation of the references to color in this figure legend, the reader is referred to the web version of this article.)

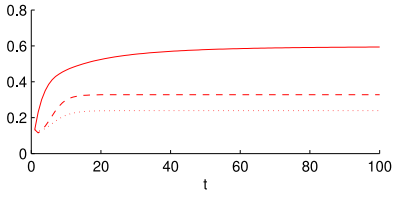

Fig. 16. The average infections for no control, Problem 1, and implementation of Algorithm 3 on Problem 2, for the systems in Fig. 15, are depicted by the solid line, dashed line, and dotted line, respectively.

This system is homogeneous in infection rate, with $\beta = 0.4592$. We compare the system with no controller (Fig. 15(a)), a controller based on solving a linear program as given in Problem 1 (Fig. 15(b)), and a controller that uses Algorithm 3 to solve Problem 2 iteratively with $\kappa = 0.05$ (Fig. 15(c)). The sums of the final probabilities of infection for all nodes ($\sum_{i=1}^{n} p_i(100)$) for the three plots are 10.7, 4.92, and 3.6, respectively. Therefore, Algorithm 3 performed best; however, both showed significant improvement over the uncontrolled simulation. The maximum eigenvalues of the three linearized systems are, from left to right, 1.893, 0.557, and 0.421; so none of the linearized systems is Hurwitz. Therefore, consistent with Theorem 1, the systems are all at an endemic state. However, even though the control efforts do not completely eradicate the virus, they do mitigate its effect (see Fig. 16). Note that in other simulations the controller obtained using the linear programming formulation (cf. Problem 1) outperformed the controller obtained by Algorithm 3 (which solves Problem 2).

8. Conclusion

We have explored a competing multi-virus SIS model through several corollaries and theorems exploring stability of the equilibria for the static graphs and mutating, time-varying graphs as well as with an awareness state. We have also proposed several control techniques that appeal to the analysis results, providing two efficient centralized antidote distribution/allocation protocols.

The results herein provide insight for real-world applications. In the context of virus spread mitigation (diseases, computer viruses, etc.), the control techniques offer insight into antidote treatment options. In the context of competing products, a marketing team could appeal to the parallel equilibrium results and try to mimic the proportion of spread parameters of their product to ensure survival.

In future work, we would like to analyze more generic cases of co-existing endemic states for the competing viruses over static graphs, endemic cycles for mutating viruses over time-varying graphs, and endemic states of competing viruses with human awareness. Many control techniques focus on changing the parameters of the model, which typically leads to more tractable algorithms. However, has been seen, e.g. with the COVID-19 pandemic, when a vaccine does not yet exist, this becomes difficult to implement. Therefore, more efforts on the removal of edges from the graph (Enns et al., 2012; Paré et al., 2018) should be considered, although this is an NP-hard problem (Mieghem et al., 2011).

Appendix. Comparison to full probabilistic model

For completeness, we provide a description of the $(m+1)^n$ state Markov model and compare to (4) via simulation; note the similarities to Liu et al. (2019) and Paré et al. (2018). Each state of the chain, $Y_\kappa(t)$, corresponds to an m-radix-valued string s of length n, where $s_i = 0$ or $s_i = k$ indicate the ith agent is, respectively, either susceptible or infected by virus $k \in [m]$. The state transition matrix, Q, is defined by

$$q_{\kappa l} = \begin{cases} \delta_i^k, & \text{if } s_i = k,\ \kappa = l + k(m+1)^{i-1} \\ \sum_{j=1}^{n} \beta_{ij}^k 1_{s_j=k}, & \text{if } s_i = 0,\ \kappa = l - k(m+1)^{i-1} \\ -\sum_{j\neq l} q_{jl}, & \text{if } \kappa = l \\ 0, & \text{otherwise,} \end{cases} \tag{A.1}$$

for $i \in [n]$. Here each virus $k \in [m]$ is propagating over a network whose infection rates are given by β_{ij}^k (nonnegative, with $\beta_{ii}^k = 0,\ \forall i, k$), δ_i^k is the associated healing rate of the ith agent, and $s_i = 0$ or $s_i = k$ indicate, respectively, the ith agent is either susceptible or infected by virus k. The state vector $y(t)$ is defined as

$$y_\kappa(t) = Pr[Y_\kappa(t) = \kappa], \tag{A.2}$$

with $\sum_{\kappa=1}^{3^n} y_\kappa(t) = 1$. The Markov chain evolves as

$$\frac{dy'(t)}{dt} = y'(t)Q. \tag{A.3}$$

Let $v_i^k(t) = Pr[X_i(t) = k]$, where $X_i(t)$ is the random variable representing whether the ith agent is susceptible or infected with one of the m viruses. Then

$$(v^k)'(t) = y'(t)M^k, \tag{A.4}$$

where the ith column of M^k indicates the states in the Markov chain where agent i is infected by virus k (all m-radix strings

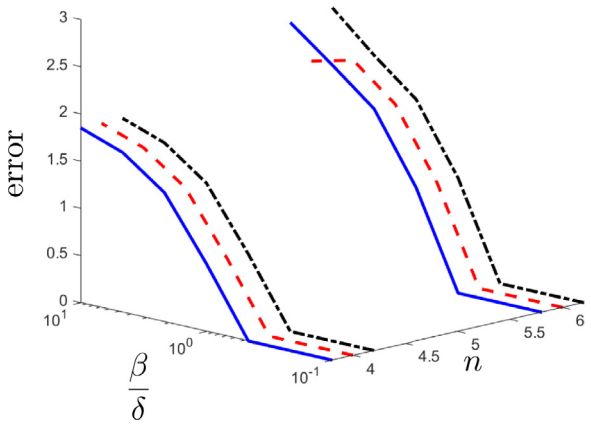

Fig. A.17. A plot of $\|[v^1(T); v^2(T); v^3(T)] - [p^1(T); p^2(T); p^3(T)]\|$ for the line graph, $T = 10{,}000$. Results from using the different initial conditions $(p^{1_1}(0), p^{2_1}(0), p^{3_1}(0))$, $(p^{1_2}(0), p^{2_2}(0), p^{3_2}(0))$, $(p^{1_3}(0), p^{2_3}(0), p^{3_3}(0))$ are depicted by the blue lines, red dashed lines, and black dash–dot lines, respectively.

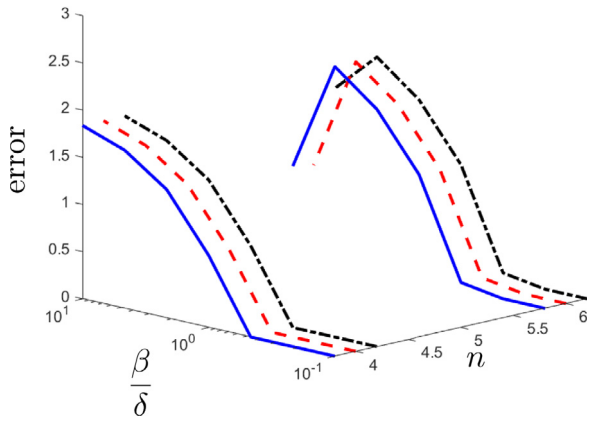

Fig. A.18. A plot of $\|[v^1(T); v^2(T); v^3(T)] - [p^1(T); p^2(T); p^3(T)]\|$ for the star graph, $T = 10{,}000$. Results from using the different initial conditions $(p^{1_1}(0), p^{2_1}(0), p^{3_1}(0))$, $(p^{1_2}(0), p^{2_2}(0), p^{3_2}(0))$, $(p^{1_3}(0), p^{2_3}(0), p^{3_3}(0))$ are depicted by the blue lines, red dashed lines, and black dash–dot lines, respectively.

where $s_i = k$), that is, $M^k = 1_{M=k}$, where $M \in \mathbb{R}^{(m+1)^n \times n}$ has rows of lexicographically-ordered m-radix numbers, bit reversed.[1] Therefore, $v_i^k(t)$ reflects the summation of all probabilities where $s_i = k$. Note that the first state of the chain, which corresponds to $s = \mathbf{0}$, the healthy state, for $\delta_i^k \ \forall i, k$, is the absorbing, or sink, state of the chain. This means that the Markov chain will never escape this state once in it, and further, since it is the only absorbing state, the system will converge to the healthy state with probability one (Norris, 1998). The model in (4) can be derived from a first-order approximation of this $(m+1)^n$ state Markov model, similar to the single-virus case (Mieghem et al., 2009).

We compare the model in (4) to the full probabilistic $(m+1)^n$ state model in (A.1)–(A.4) via simulations to illustrate the effectiveness of the approximation. We set $m = 3$, and use line graphs, star (hub–spoke) graphs, and complete graphs. All adjacency matrices for these graphs are symmetric and binary-valued, and both viruses spread over the same graph. In the star graph, the central node is the first agent. Each simulation was run for 10,000 time steps (final time $T = 10{,}000$), with three initial conditions: (1) the first, second, and third nodes are infected by virus 1, virus 2, and virus 3, respectively, $p^{1_1}(0) = [1\ 0\ \cdots\ 0]^\top$, $p^{2_1}(0) = [0\ 1\ 0\ \cdots\ 0]^\top$, $p^{3_1}(0) = [0\ 0\ 1\ 0\ \cdots\ 0]^\top$; (2) the first two nodes are infected by virus 1 and the third and fourth nodes are infected by viruses 2 and 3, respectively, $p^{1_2}(0) = [1\ 1\ 0\ \cdots\ 0]^\top$, $p^{2_2}(0) = [0\ 0\ 1\ 0\ \cdots\ 0]^\top$, $p^{3_2}(0) = [0\ 0\ 0\ 1\ 0\ \cdots\ 0]^\top$; and (3) the first and second nodes are infected by viruses 1 and 2, respectively, and the remaining nodes are infected by virus 3, $p^{1_3}(0) = [1\ 0\ 0\cdots\ 0]^\top$, $p^{2_3}(0) = [0\ 1\ 0\ \cdots\ 0]$, $p^{2_3}(0) = [0\ 0\ 1\ \cdots\ 1]$. In these tests we explore identical homogeneous viruses, $(\beta, \delta) = (\beta^1, \delta^1) = (\beta^2, \delta^2) = (\beta^3, \delta^3)$. The (β, δ) pairs are $[(0.1, 1), (0.215, 1), (0.464, 1), (0.5, 0.5), (1, 0.464), (1, 0.215), (1, 0.1)]$, and the numbers of agents are $n = 4, 6$. We limited simulations to these n values since mean field approximations are typically worse for small values of n and there is a computational limitation due to the size of the $(m+1)^n$ state model.

The results are given in Figs. A.17–A.19 in terms of the 2-norm of the difference between the states of (5) at the final time ($[p^1(T); p^2(T); p^3(T)]$), and the means of the $m = 3$ viruses in the $(m+1)^n$ state Markov model at the final time ($[v^1(T); v^2(T); v^3(T)]$ as defined by (A.4)).

The accuracy of the approximation appears to be very similar to the single virus case (Mieghem et al., 2009; Paré et al., 2018)

[1] Matlab code: $M = fliplr(dec2base(0:((m+1)^n)-1, m+1) - '0')$

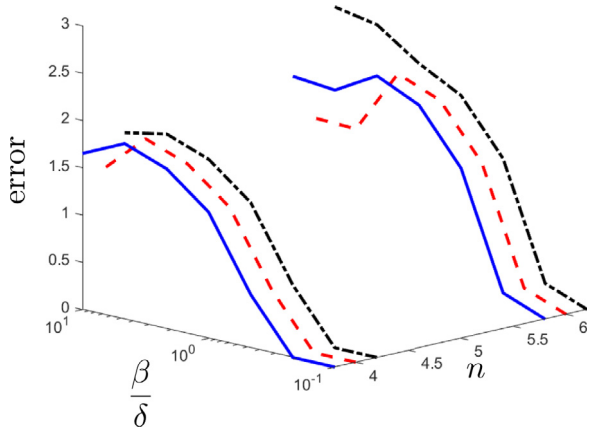

Fig. A.19. A plot of the error $\|[v^1(T); v^2(T); v^3(T)] - [p^1(T); p^2(T); p^3(T)]\|$ for the complete graph, $T = 10{,}000$. Results from using the different initial conditions $(p^{1_1}(0), p^{2_1}(0), p^{3_1}(0))$, $(p^{1_2}(0), p^{2_2}(0), p^{3_2}(0))$, $(p^{1_3}(0), p^{2_3}(0), p^{3_3}(0))$ are depicted by the blue lines, red dashed lines, and black dash–dot lines, respectively.

and to the two-virus case (Liu et al., 2019). Since (5) is an upper bounding approximation, the results show that the two models converge to the healthy state for the smaller values of $\frac{\beta}{\delta}$, resulting in small errors between the two models. For many of the larger values of $\frac{\beta}{\delta}$, (5) again performs well since it is at an epidemic state and the $(m+1)^n$ state model does not appear to reach the healthy state in the finite time considered in the simulations ($T = 10{,}000$). Therefore for certain values of $\frac{\beta}{\delta}$ and certain time scales, (5) is a sufficient approximation of the $(m+1)^n$ state Markov model. For values of $\frac{\beta}{\delta}$ that are near 1, the models are notably different, similar to the single- and two-virus cases. The $(m+1)^n$ state model appears, in most cases, to be at or close to the healthy state while (5) is at an endemic state, resulting in large errors.

References

Ahn, H. J., & Hassibi, B. (2013). Global dynamics of epidemic spread over complex networks. In *Proc. 52nd IEEE Conf. Decision and Control* (pp. 4579–4585).

Ahn, Y. Y., Jeong, H., Masuda, N., & Noh, J. D. (2006). Epidemic dynamics of two species of interacting particles on scale-free networks. *Physical Review E, 74*(6), Article 066113.

Bernoulli, D. (1760). Essai d'une nouvelle analyse de la mortalité causée par la petite vérole et des avantages de l'inoculation pour la prévenir. *Histoire de l'Académie Royale Science (Paris) avec Mémories des Mathématique et Physique and Mémories*, 1–45.

Bokharaie, V. S., Mason, O., & Wirth, F. (2010). Spread of epidemics in time-dependent networks. In *Proc. 19th International Symposium on Mathematical Theory of Networks and Systems* (pp. 1717–1719).

Candes, E. J., Wakin, M. B., & Boyd, S. P. (2008). Enhancing sparsity by reweighted ℓ_1 minimization. *Journal of Fourier Analysis and Applications*, *14*(5–6), 877–905.

Daubechies, I., DeVore, R., Fornasier, M., & Güntürk, C. S. (2010). Iteratively reweighted least squares minimization for sparse recovery. *Communications on Pure and Applied Mathematics*, *63*(1), 1–38.

Dong, E., Du, H., & Gardner, L. (2020). An interactive web-based dashboard to track COVID-19 in real time. *The Lancet Infectious Diseases*, *20*(5), 533–534.

Enns, E. A., Mounzer, J. J., & Brandeau, M. L. (2012). Optimal link removal for epidemic mitigation: A two-way partitioning approach. *Mathematical Biosciences*, *235*(2), 138–147.

Fall, A., Iggidr, A., Sallet, G., & Tewa, J.-J. (2007). Epidemiological models and Lyapunov functions. *Mathematical Modelling of Natural Phenomena*, *2*(1), 62–68.

Fefferman, N. H., & Ng, K. L. (2007). How disease models in static networks can fail to approximate disease in dynamic networks. *Physical Review E*, *76*(3), Article 031919.

Funk, S., Gilad, E., Watkins, C., & Jansen, V. A. A. (2009). The spread of awareness and its impact on epidemic outbreaks. *Proceedings of the National Academy of Sciences*, *106*, 6872–6877.

Funk, S., & Jansen, V. A. A. (2010). Interacting epidemics on overlay networks. *Physical Review E*, *81*(3), Article 036118.

Granell, C., Gómez, S., & Arenas, A. (2013). Dynamical interplay between awareness and epidemic spreading in multiplex networks. *Physical Review Letters*, *111*, Article 128701.

Gubar, E., & Zhu, Q. (2013). Optimal control of influenza epidemic model with virus mutations. In *Proc. European Control Conf.* (pp. 3125–3130).

Horn, R. A., & Johnson, C. R. (2012). *Matrix analysis*. Cambridge Univ. Press.

Karrer, B., & Newman, M. E. J. (2011). Competing epidemics on complex networks. *Physical Review E*, *84*(3), Article 036106.

Kermack, W., & McKendrick, A. G. (1932). Contributions to the mathematical theory of epidemics. II. The problem of endemicity. *Proceedings of the Royal Society*, *138*(834), 55–83.

Khalil, H. K. (1996). *Nonlinear systems*. Prentice Hall.

Khanafer, A., Başar, T., & Gharesifard, B. (2014). Stability properties of infected networks with low curing rates. In *Proc. American Control Conf., 2014* (pp. 3579–3584).

Khanafer, A., Başar, T., & Gharesifard, B. (2016). Stability of epidemic models over directed graphs: a positive systems approach. *Automatica*, *74*, 126–134.

Kutch, J. J., & Gurfil, P. (2002). Optimal control of HIV infection with a continuously-mutating viral population. In *Proc. American Control Conf.* (vol. 5). (pp. 4033–4038).

Lai, M. J., Xu, Y., & Yin, W. (2013). Improved iteratively reweighted least squares for unconstrained smoothed ℓ_q minimization. *SIAM Journal of Numerical Analysis*, *51*(2), 927–957.

Lewnard, J. A., & Lo, N. C. (2020). Scientific and ethical basis for social-distancing interventions against COVID-19. *The Lancet Infectious Diseases*, *20*(6), 631.

Liu, J., Paré, P. E., Nedić, A., Beck, C. L., & Başar, T. (2017). On a continuous-time multi-group bi-virus model with human awareness. In *Proc. 56th Conf. Decision and Control* (pp. 4124–4129).

Liu, J., Paré, P. E., Nedić, A., Tang, C. Y., Beck, C. L., & Başar, T. (2016). On the analysis of a continuous-time bi-virus model. In *Proc. 55th IEEE Conf. Decision and Control* (pp. 290–295).

Liu, J., Paré, P. E., Nedić, A., Tang, C. T., Beck, C. L., & Başar, T. (2019). Analysis and control of a continuous-time bi-virus model. *IEEE Transactions on Automatic Control*, *64*(12), 4891–4906.

Mieghem, P. V., Omic, J., & Kooij, R. (2009). Virus spread in networks. *IEEE/ACM Transactions on Networking*, *17*(1), 1–14.

Mieghem, P. V., Stevanović, D., Kuipers, F., Li, C., Bovenkamp, R. V. D., Liu, D., & Wang, H. (2011). Decreasing the spectral radius of a graph by link removals. *Physical Review E*, *84*(1), 016101.

Norris, J. R. (1998). *Markov chains*. Cambridge Univ. Press.

Nowak, M. (1991). The evolution of viruses: Competition between horizontal and vertical transmission of mobile genes. *Journal of Theoretical Biology*, *150*(3), 339–347.

Ogura, M., & Preciado, V. M. (2016). Epidemic processes over adaptive state-dependent networks. *Physical Review E*, *93*, Article 062316.

Paarporn, K., Eksin, C., Weitz, J. S., & Shamma, J. S. (2017). Networked SIS epidemics with awareness. *IEEE Transactions on Computational Social Systems*, *4*(3), 93–103.

Paré, P. E., Beck, C. L., & Nedić, A. (2015). Stability analysis and control of virus spread over time–varying networks. In *Proc. 54th IEEE Conf. Decision and Control* (pp. 3554–3559).

Paré, P. E., Beck, C. L., & Nedić, A. (2016). Epidemic processes over time–varying networks. arXiv:1609.05128v1 [math.OC], arXiv.

Paré, P. E., Beck, C. L., & Nedić, A. (2018). Epidemic processes over time–varying networks. *IEEE Transactions on Control of Network Systems*, *5*(3), 1322–1334.

Paré, P. E., Liu, J., Beck, C. L., Nedić, A., & Başar, T. (2017). Multi-competitive viruses over static and time–varying networks. In *Proc. American Control Conf.* (pp. 1685–1690).

Pasqualetti, F., Zampieri, S., & Bullo, F. (2014). Controllability metrics, limitations and algorithms for complex networks. *IEEE Transactions on Control of Network Systems*, *1*(1), 40–52.

Peng, C., Jin, X., & Shi, M. (2010). Epidemic threshold and immunization on generalized networks. *Physica A: Statistical Mechanics and its Applications*, *389*(3), 549–560.

Prakash, B., Beutel, A., Rosenfeld, R., & Faloutsos, C. (2012). Winner takes all: Competing viruses or ideas on fair-play networks. In *Proc. 21st International Conf. World Wide Web* (pp. 1037–1046).

Prakash, B. A., Tong, H., Valler, N., Faloutsos, M., & Faloutsos, C. (2010). Virus propagation on time-varying networks: Theory and immunization algorithms. In *Machine Learning and Knowledge Discovery in Databases* (pp. 99–114). Springer.

Preciado, V., Zargham, M., Enyioha, C., Jadbabaie, A., & Pappas, G. (2014). Optimal resource allocation for network protection against spreading processes. *IEEE Transactions on Control of Network Systems*, *1*(1), 99–108.

Rami, M. A., Bokharaie, V. S., Mason, O., & Wirth, F. R. (2014). Stability criteria for SIS epidemiological models under switching policies. *Discrete and Continuous Dynamical Systems Series*, *19*(9), 2865–2887.

Sahneh, F., & Scoglio, C. (2011). Epidemic spread in human networks. In *Proc. 50th IEEE Conf. Decision and Control* (pp. 3008–3013).

Sahneh, F., & Scoglio, C. (2012). Optimal information dissemination in epidemic networks. In *Proc. 51st IEEE Conf. Decision and Control* (pp. 1657–1662).

Sahneh, F. D., & Scoglio, C. (2014). Competitive epidemic spreading over arbitrary multilayer networks. *Physical Review E*, *89*(6), Article 062817.

Santos, A., Moura, J. M. F., & Xavier, J. M. F. (2015). Bi-virus SIS epidemics over networks: Qualitative analysis. *IEEE Transactions on Network Science and Engineering*, *2*(1), 17–29.

Schwarzkopf, Y., Rákos, A., & Mukamel, D. (2010). Epidemic spreading in evolving networks. *Physical Review E*, *82*(3), Article 036112.

Shakeri, H., Sahneh, F. D., Scoglio, C., Poggi-Corradini, P., & Preciado, V. M. (2015). Optimal information dissemination strategy to promote preventive behaviors in multilayer epidemic networks. *Mathematical Bioscience and Engineering*, *12*(3), 609–623.

Singh, N. (2006). *Epidemiological models for mutating pathogens with temporary immunity* (Ph.D. thesis), Univ. of Central Florida.

Solo, V. (1994). On the stability of slowly time-varying linear systems. *Mathematics of Control, Signals and Systems*, *7*(4), 331–350.

Vijayshankar, A., & Roy, S. (2012). Cost of fairness in disease spread control. In *Proc. 51st IEEE Conf. Decision and Control* (pp. 4930–4935).

Volz, E., & Meyers, L. A. (2009). Epidemic thresholds in dynamic contact networks. *Journal of the Royal Society Interface*, *6*(32), 233–241.

Wan, Y., Roy, S., & Saberi, A. (2007). Network design problems for controlling virus spread. In *Proc. 46th IEEE Conf. Decision and Control* (pp. 3925–3932).

Wan, Y., Roy, S., & Saberi, A. (2008). Designing spatially heterogeneous strategies for control of virus spread. *IET Systems Biology*, *2*(4), 184–201.

Wang, Y., Chakrabarti, D., Wang, C., & Faloutsos, C. (2003). Epidemic spreading in real networks: An eigenvalue viewpoint. In *Proc. 22nd International Symposium on Reliable Distributed Systems* (pp. 25–34).

Watkins, N. J., Nowzari, C., Preciado, V. M., & Pappas, G. J. (2016). Optimal resource allocation for competitive spreading processes on bilayer networks. *IEEE Transactions on Control of Network Systems*, *5*(1), 298–307.

Wei, X., Valler, N. C., Prakash, B. A., Neamtiu, I., Faloutsos, M., & Faloutsos, C. (2013). Competing memes propagation on networks: A network science perspective. *IEEE Journal on Selected Areas in Communications*, *31*(6), 1049–1060.

Wright, J., Ganesh, A., Rao, S., Peng, Y., & Ma, Y. (2009). Robust principal component analysis: Exact recovery of corrupted low-rank matrices via convex optimization. In *Advances in Neural Information Processing Systems* (pp. 2080–2088).

Xu, S., Lu, W., & Zhan, Z. (2012). A stochastic model of multivirus dynamics. *IEEE Transactions on Dependable and Secure Computing*, *9*(1), 30–45.

Yagan, O., Qian, D., Zhang, J., & Cochran, D. (2013). Conjoining speeds up information diffusion in overlaying social-physical networks. *IEEE Journal on Selected Areas in Communications*, *31*(6), 1038–1048.

Philip E. Paré is an Assistant Professor in the School of Electrical and Computer Engineering at Purdue University. He received his Ph.D. in Electrical and Computer Engineering from the University of Illinois at Urbana–Champaign in 2018, after which he went to KTH Royal Institute of Technology in Stockholm, Sweden to be a Post-Doctoral Scholar from 2019 to 2020. He received his B.S. in Mathematics with University Honors and his M.S. in Computer Science from Brigham Young University in 2012 and 2014, respectively. At the University of Illinois, he was the recipient of the Robert T. Chien Memorial Award for excellence in research and named a Mavis Future Faculty Fellow. His research focuses on networked control systems, namely modeling, analysis, and control of virus spread over networks.

Ji Liu received the B.S. degree in information engineering from Shanghai Jiao Tong University, Shanghai, China, in 2006, and the Ph.D. degree in electrical engineering from Yale University, New Haven, CT, USA, in 2013. He is currently an Assistant Professor in the Department of Electrical and Computer Engineering at Stony Brook University, Stony Brook, NY, USA. Prior to joining Stony Brook University, he was a Postdoctoral Research Associate at the Coordinated Science Laboratory, University of Illinois at Urbana–Champaign, Urbana, IL, USA, and the school of Electrical, Computer and Energy Engineering at Arizona State University, Tempe, AZ, USA. His current research interests include distributed control and optimization, distributed machine learning, multi-agent systems, epidemic networks, social networks, and cyber–physical systems.

Carolyn L. Beck is a professor at the University of Illinois, Urbana–Champaign (UIUC) in the Industrial and Enterprise Systems Engineering (ISE) Department. She completed her Ph.D. at Caltech, her M.S. at Carnegie Mellon, and her B.S. at Cal Poly, all in Electrical Engineering. Prior to completing her Ph.D., she worked at Hewlett-Packard in Silicon Valley, designing digital hardware and software for measurement instruments. She has held visiting faculty positions at the Royal Institute of Technology (KTH) in Stockholm, Stanford University in Palo Alto and Lund University in Lund, Sweden. She has received national research awards and local teaching awards. Prof. Beck's research interests range from network inference problems to control of anesthetic pharmacodynamics. Her main research interests are in mathematical modeling, analysis and control of network systems; model reduction and approximation; and clustering and aggregation methods applied to data from network systems.

Angelia Nedić has a Ph.D. from Moscow State University, Moscow, Russia, in Computational Mathematics and Mathematical Physics (1994), and a Ph.D. from Massachusetts Institute of Technology, Cambridge, USA in Electrical and Computer Science Engineering (2002). She has worked as a senior engineer in BAE Systems North America, Advanced Information Technology Division at Burlington, MA. Currently, she is a faculty member of the school of Electrical, Computer and Energy Engineering at Arizona State University at Tempe. Prior to joining Arizona State University, she has been a Willard Scholar faculty member at the University of Illinois at Urbana–Champaign. She has been a recipient of NSF CAREER Award 2007 in Operations Research for her work in distributed multi-agent optimization. She is a recipient (jointly with her co-authors) of the Best Paper Award at the Winter Simulation Conference 2013 and the Best Paper Award at the International Symposium on Modeling and Optimization in Mobile, Ad Hoc and Wireless Networks (WiOpt) 2015. Her general research interest is in large scale complex systems dynamics and optimization.

Tamer Başar is with the University of Illinois at Urbana–Champaign (UIUC), where he holds the academic positions of Swanlund Endowed Chair; Center for Advanced Study Professor of Electrical and Computer Engineering; Research Professor at the Coordinated Science Laboratory; and Research Professor at the Information Trust Institute. He is also the Director of the Center for Advanced Study. He received B.S.E.E. from Robert College, Istanbul, and M.S., M.Phil, and Ph.D. from Yale University. He is a member of the US National Academy of Engineering, and Fellow of IEEE, IFAC and SIAM, and has served as president of IEEE CSS, ISDG, and AACC. He has received several awards and recognitions over the years, including the highest awards of IEEE CSS, IFAC, AACC, and ISDG; the IEEE Control Systems Award; and a number of international honorary doctorates and professorships. He has over 900 publications in systems, control, communications, and dynamic games, including books on non-cooperative dynamic game theory, robust control, network security, wireless and communication networks, and stochastic networked control. He was the Editor-in-Chief of Automatica between 2004 and 2014, and is currently editor of several book series. His current research interests include stochastic teams, games, and networks; security; and cyber–physical systems.